AD-A065 551 BOSTON UNIV MASS DEPT OF ASTRONOMY F/G 4/1
FINITE ELEMENT SIMULATION OF PROCESSES IN THE AURORAL IONOSPHER--ETC(U)
JAN 79 B VANCE, M MENDILLO F19628-78-C-0079
UNCLASSIFIED ACBU-SER-III-NO-12 AFGL-TR-79-0003 NL

1 OF 2
AD
AD A065551

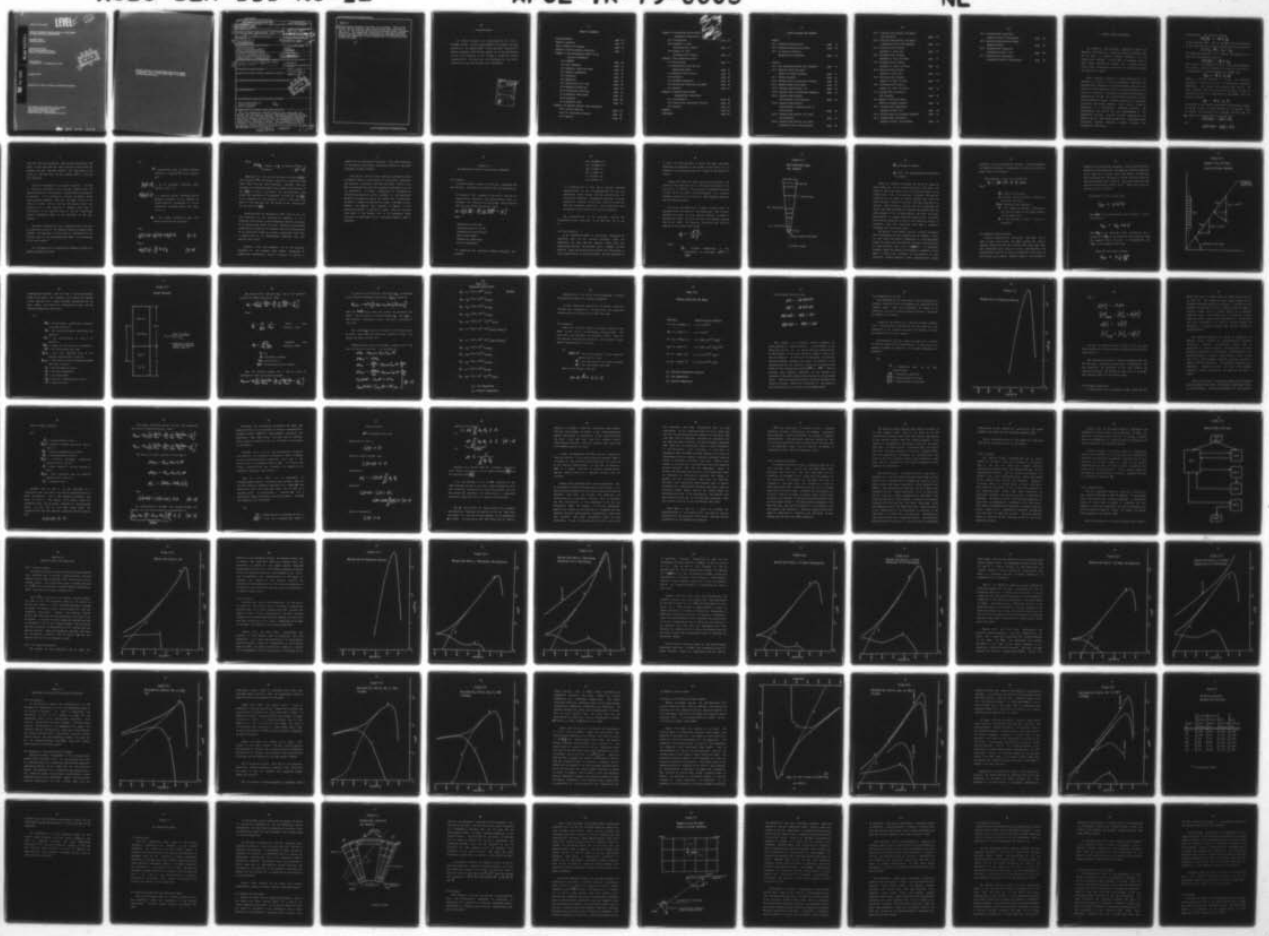

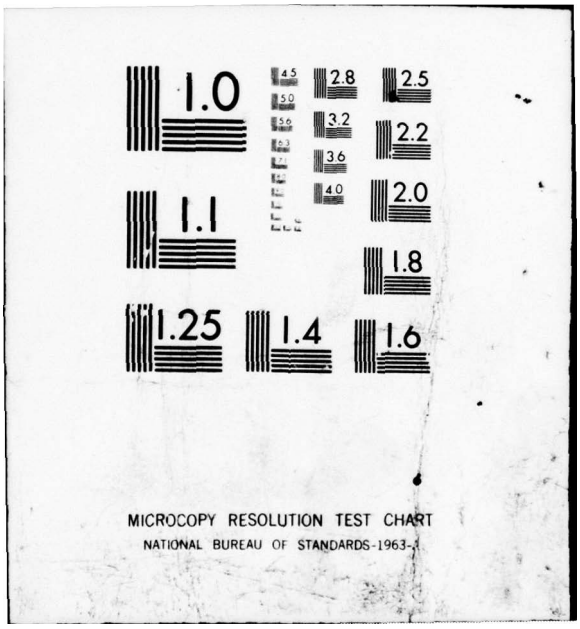
1.0
1.1
1.25
1.4
1.6
1.8
2.0
2.2
2.5
2.8
3.2
3.6
4.0
4.5
5.0
5.6
MICROCOPY RESOLUTION TEST CHART
NATIONAL BUREAU OF STANDARDS-1963-A

AFGL-TR-79-0003

LEVEL II

12

FINITE ELEMENT SIMULATION OF PROCESSES IN THE AURORAL IONOSPHERE

Bradley Vance
Michael Mendillo

Boston University
881 Commonwealth Avenue
Boston, Massachusetts 02215

Final Report
1 October 1977 - 30 September 1978

January 1979

Approved for public release; distribution unlimited

AIR FORCE GEOPHYSICS LABORATORY
AIR FORCE SYSTEMS COMMAND
UNITED STATES AIR FORCE
HANSCOM AFB, MASSACHUSETTS 01731

Unclassified

SECURITY CLASSIFICATION OF THIS PAGE (When Data Entered)

REPORT DOCUMENTATION PAGE

READ INSTRUCTIONS BEFORE COMPLETING FORM

1. REPORT NUMBER: AFGL-TR-79-0003	2. GOVT ACCESSION NO.
3. RECIPIENT'S CATALOG NUMBER	
4. TITLE (and Subtitle): FINITE ELEMENT SIMULATION OF PROCESSES IN THE AURORAL IONOSPHERE.	5. TYPE OF REPORT & PERIOD COVERED: Final rept. 1 October 1977-30 September 1978
6. PERFORMING ORG. REPORT NUMBER: A.C.B.U., Ser. III, no. 12	
7. AUTHOR(s): Bradley Vance, Michael Mendillo	8. CONTRACT OR GRANT NUMBER(s): F19628-78-C-0079
9. PERFORMING ORGANIZATION NAME AND ADDRESS: Boston University, 881 Commonwealth Avenue, Boston, Massachusetts 02215	10. PROGRAM ELEMENT, PROJECT, TASK AREA & WORK UNIT NUMBERS: 61102F, DMSP00AD
11. CONTROLLING OFFICE NAME AND ADDRESS: Air Force Geophysics Laboratory, Hanscom AFB, Massachusetts 01731, Monitor/Peter J.L. Wildman/PHR	12. REPORT DATE: January 1979; 13. NUMBER OF PAGES
14. MONITORING AGENCY NAME & ADDRESS (if different from Controlling Office): ACBU-SER-III-NO-12	15. SECURITY CLASS. (of this report): Unclassified; 15a. DECLASSIFICATION/DOWNGRADING SCHEDULE

16. DISTRIBUTION STATEMENT (of this Report)

Approved for public release; distribution unlimited

113 p.

17. DISTRIBUTION STATEMENT (of the abstract entered in Block 20, if different from Report)

DDC RECEIVED MAR 12 1979 C

18. SUPPLEMENTARY NOTES

19. KEY WORDS (Continue on reverse side if necessary and identify by block number)

Finite Element Simulation
Numerical Simulation
Auroral Ionosphere
Cusp
Trough

20. ABSTRACT (Continue on reverse side if necessary and identify by block number)

A two dimensional computer model of the night-time ionosphere was developed to simulate atmospheric processes acting at mid and high latitude regions. The computational method used was finite element simulation (FES) of the physical processes rather than a numerical solution of the differential equations governing the ionospheric system. The processes of O+ and H+ transport, several chemical reactions and O+ production due to

DD FORM 1 JAN 73 1473 EDITION OF 1 NOV 65 IS OBSOLETE

406311

Unclassified

(over)

BLOCK 20

precipitating energetic electrons were included. The initial neutral and ion profiles were input and the time evolution of the O+, H+, NO+ and O_2^+ profiles were simulated using a suitable time step. One dimensional simulations of the winter dayside auroral cusp and night-time Millstone Hill profiles and a two dimensional simulation of the poleward wall of the mid-latitude trough were made.

Acknowledgement

We wish to express our appreciation to Dr. P.J.L. Wildman of AFGL for his encouragement and support for this project; to Dr. Bohdan Balko of the National Institute of Health, Bethesda, Maryland who guided us in the application of the FES technique; to Dr. Chacko C. Chacko of Boston University for his help with the simulation of the winter dayside cusp and the poleward wall ionospheres.

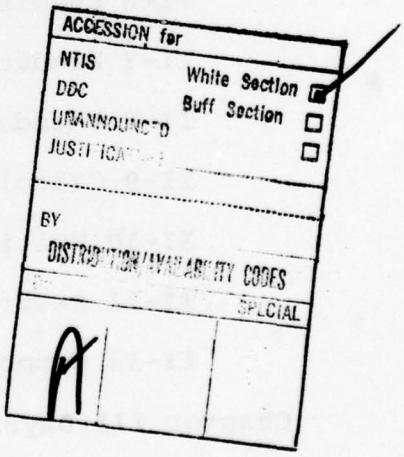

TABLE OF CONTENTS

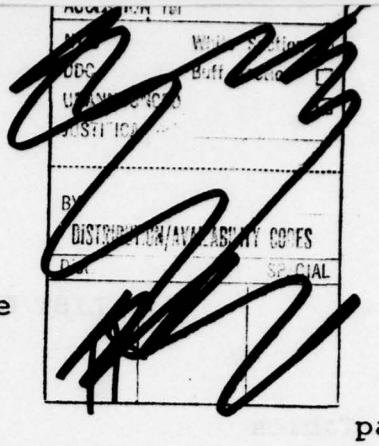

LIST OF TABLES AND FIGURES

Tables

Figures

I FINITE ELEMENT SIMULATION

The method of Finite Element Simulation, (Balko and Mendillo, 1977) FES, is a powerful numerical technique that may be used to simulate physical processes in very complicated systems. In fact, FES is sometimes able to give useful quantitative results for a given physical system, when conventional analytical and numerical methods are difficult to apply.

When a physical problem is solved analytically, the approach is to write a set of differential equations that mathematically represents the physical model and then to use some well known analytical method or educated guess work to arrive at a solution. Often when the analytical approach is unsuccessful the same set of differential equations can be solved numerically using a proven technique or a synthesis of several well known methods. In the case of either an analytical or a conventional numerical solution, the investigator must usually be very knowledgeable of the mathematics involved, and this is more important as the physical system under study becomes more complicated since increasing physical complexity greatly increases the mathematical complexity.

being studied, the familiar equation

$$dC_2/dt = -k\, C_1 \cdot C_2$$

is the starting point. Here C_1 and C_2 are the concentrations of the reactants and k is the reaction rate of the reaction:

$$C_1 + C_2 \xrightarrow{k} C_3 + C_4$$

The analytical approach is to integrate this equation or to write the complementary equation

$$dC_1/dt = -k\, C_1 \cdot C_2$$

and to solve this system of coupled first order equations. In a typical numerical approach the system of two equations is descretized by letting $dC \rightarrow \Delta C$ and $dt \rightarrow \Delta t$. Then

$$\Delta C_2 = -k\, C_1 \cdot C_2 \cdot \Delta t$$

Though in the FES technique it is not, in principle, necessary to write out the set of differential equations explicitly, this example is so simple that FES is, in fact, starting with the differential equations. It must be stressed that this is a consequence of the example. Once the descrete relation

$$\Delta C = -k\, C_1 \cdot C_2\, \Delta t$$

is arrived at and initial conditions are deteremined, namely C_1 and C_2 at t=0, the FES technique can be applied. That is, choose an appropriate time step Δt, calculate ΔC_1 and ΔC_2, update the concentrations C_1 and C_2 so that

$$C_1(t+\Delta t) = C_1(t) + \Delta C_1$$

and

$$C_2(t+\Delta t) = C_2(t) + \Delta C_2$$

and proceed to the next time step and calculate in a like manner. This is continued as long as desired.

The above example provides a capsule summary of the basic components of the FES technique. These are:

1. Write down the basic equations relating the physical parameters of the system. It is not necessary to explicitly write down an overall set of differential equations governing the system.

2. Descretize the basic equations as necessary.

3. Choose an appropriate time step. (An important point to be discussed more fully in Chapter II.)

4. Begin the simulation from the initial conditions.

5. Determine the end point of the simulation, e.g. some particular time or a particular value of one of the parameters being studied.

This summary suggests that FES is most applicable to initial value problems. This is the case. FES is very useful for problems where the initial values of a set of parameters are known and their evolution in time is to be

studied.

It is very important to point out the key assumptions that are fundamental in this FES technique.

1. It is valid during an appropriately chosen time step, to treat processes that may be non-linearly coupled in a linear fashion, i.e., during the simulation, to allow a physical process to operate as though it were the only one, then proceed to the next process and treat that in a like manner and to continue until all processes have been calculated within one time step.

2. It is possible to determine an appropriate time step (which will fix the time grid) and to determine an appropriate spatial grid.

3. It is possible to monitor the error in such a descretized calculation in some quantitative way.

The first of these assumptions is warranted if the time step and the spatial grid are of appropriate size. In fact, there are two ways of handling the updating of the parameters. Each parameter may be updated after each process within a time step, or all parameters may be updated

only once after all processes have operated during the time step. If the time step has been correctly chosen these two methods will give the same results. The importance of the choice of the time step and the spatial grid is now even more apparent.

The second assumption is the most critical. In order to choose an appropriate time step and spatial grid the specific details of the physical system must be considered. In general, it is possible to do this by making common sense physical arguments that will put upper limits on the size of the time step as well as the spatial grid. The selection of a time step and a spatial grid will be illustrated in the specific case of the one dimensional auroral ionosphere model to be discussed in the next chapter.

The final assumption is also important and it too must be justified in view of the specific physical problem being studied. The question of error will be considered for the specific case of the one dimensional model to be discussed in the next chapter.

It is possible now to express the technique of FES in a general mathematical form.

Let

$\vec{r}'$ = some volume, area, or linear interval centered at location $\vec{r}$ in the spatial grid

$\{Q_j(\vec{r}', t)\}$ = set of dependent variables being studied, j=1,2,...m

$P_i(\{Q_j\}, \vec{r}', t)$ = a physical process relating various dependent variables to one another, to various physical parameters, or to the independent variables space and time; i=1,2,...n

Δt = the chosen calculation time step which determines the time grid

Then:

$$Q_j(\vec{r}', t+\Delta t) = Q_j(\vec{r}', t) + \Delta Q_j(\vec{r}', t) \qquad (I-1)$$

Where

$$\Delta Q_j(\vec{r}', t) = \sum_{i=1}^{m} P_i * Q_j \qquad (I-2)$$

Where

$P_i * Q_j$ = change in Q_j at location $\vec{r}'$ due to process i (I - 3)

Equations I-1, I-2, and I-3 are used to calculate $\{Q_j\}$ at all locations $\vec{r}'$ of the spatial grid for a particular time step. When this has been completed, the next time step proceeds in an identical manner and thereby the evolution of the $\{Q_j\}$ in time is calculated. At any particular time during the simulation it is possible to print out the $\{Q_j\}$. It is necessary for the computer code to store only one point of the time grid and all points of the spatial grid for the values of $\{Q_j\}$.

Recapitulating the advantages of FES, first of all, and very important to the scientist or engineer, it is a technique that focuses on the fundamental physical processes of the system under study. The basic physical relationships involving the parameters of interest form the starting point of the simulation. There is no need to explicitly write down a complicated set of differential equations that will describe the system.

Secondly, since the emphasis is on the physical processes of the problem, they remain unobscured by complicated mathematical details involved in solving a

complex set of differential equations. This high visibility of the physics makes adding additional physics to the model extremely straight forward.

And finally, there are many physical problems in which an adequate model is untractable to conventional analytical and numerical techniques (Hastings and Roble, 1977). Since FES is concerned with the basic physical processes it is not as susceptible to being overwhelmed by mathematical difficulties presented by the problem. If the individual physical processes are known, the model can, in principle, be made as complex as desired and remain tractable to FES. However, the computer time required to simulate a very complicated system by FES may be great. This is the main draw back of the method, but it is constantly being diminished in importance by the increasing speed of today's computers.

Chapter II

One Dimensional Model of the Auroral Ionoshpere

II-1 Summary

A one dimensional model of the auroral ionosphere has been devised. The physical processes that are included are:

a) Transport: The transport of O+ and H+ ions due to concentration gradients and gravitational drift is included. The equation for the plasma drift velocity that was used (Banks and Holzer, 1969):

$$u = D\left[\frac{1}{C}\frac{\partial C}{\partial z} + \frac{T_e}{T_i}\frac{1}{n(e)}\frac{\partial n(e)}{\partial z} + \frac{1}{H}\right]$$

Where

D=Diffusion coefficient

C=Concentration of the ion

n(e)=Electron concentration

H=Ion scale height

Te=Electron temperature

Ti= Ion temperature

b) Chemistry: The following chemical reactions are included:

$$N_2 + O^+ \longrightarrow NO^+ + O$$

$$O_2 + O^+ \longrightarrow O_2^+ + O$$

$$NO^+ + e \longrightarrow N + O$$

$$O_2^+ + e \longrightarrow O + O$$

$$H + O^+ \longrightarrow O + H^+$$

$$H^+ + O \longrightarrow O^+ + H$$

c) Production of O^+ ions due to auroral electron precipitation. In the two applications of the one dimensional model (winter day side auroral cusp and mid-latitude nightime ionospheres) there was no solar production. However, if the model were to be used for day time ionosphere simulation, solar production could be handled in the same way as auroral production.

The concentrations of the following species are calculated at each time step: e, O^+, NO^+, O_2^+, H^+, O, and H.

II-2 Cell Geometry

A one dimensional model of the auroral ionosphere is justified since at the auroral latitudes where the simulation has been made the magnetic field lines are essentially vertical and parallel up to a height of over 2000 km. Since the plasma is held within the field lines, a first approximation is justified where the cell geometry is

a stack of cells for each of which the upper and lower boundaries are parallel to the surface of the earth, i.e., a segment of a circle drawn with the center of the earth as a center.

Figure II-1 shows the shape and size of the boxes. The center of the lowest box is at 150 km and the center of the top box is at 2010 km. The reason for extending the boxes to 2010 km is to enable the establishment of a suitable boundary condition at the top cell. This boundary condition will be discussed later.

The cross sectional area of these vertical cells is arbitrary since the model is one dimensional. The vertical dimension is chosen to be as large as possible in order to minimize the number of cells and thus the computer running time of the model. The limit on the size of the cells is imposed by the plasma scale height

$$H_p = \frac{k T_p}{m g}$$

Where

T_p = electron temperature + ion temperature, in this model 2000° K + 1000°K

FIGURE II-1

ONE DIMENSIONAL MODEL
CELL GEOMETRY

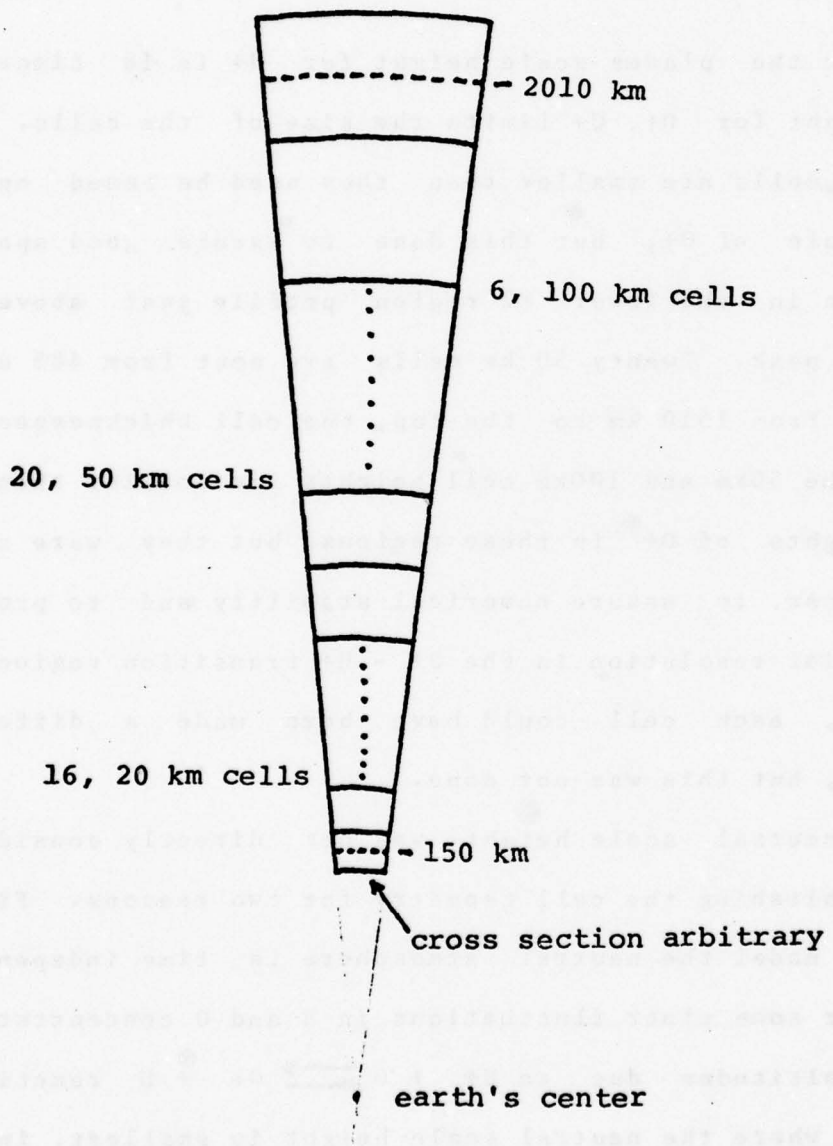

k = Boltzman's constant

g = g(z), the gravitational acceleration at height z

Since the plasma scale height for H+ is 16 times the scale height for O+, O+ limits the size of the cells. The lower 16 cells are smaller than they need be based on the plasma scale of O+, but this done to assure good spatial resolution in the lower F2 region profile just above and below the peak. Twenty 50 km cells are next from 485 up to 1435 km. From 1510 km to the top, the cell thicknesses are 100 km. The 50km and 100km cell heights are smaller than the scale heights of O+ in these regions but they were used, nevertheless, to assure numerical stability and to provide good spatial resolution in the O+ - H+ transition region. In principle, each cell could have been made a different thickness, but this was not done.

The neutral scale height was not directly considered when establishing the cell geometry for two reasons. First, in this model the neutral atmosphere is time independent except for some minor fluctuations in H and O concentrations at high altitudes due to $H^+ + O \rightleftharpoons O^+ + H$ reactions. Secondly, where the neutral scale height is smallest, in the lower F region, the influence of the neutrals is felt indirectly through chemistry which dominates over plasma

transport as the most important process. The FES treatment of chemical processes is independent of cell size as will be shown later in the chapter.

The volume of a cell i is calculated by

$$V_i = (Re + H) \cdot Z \cdot \theta \cdot 1cm$$

where

Re = radius of the earth

H = height above the earth's surface of the center of cell i

$1cm$ = arbitrary cell thickness

θ = the angle (in radians) subtended at the earth's center by the lower boundary of the lowest cell

Z = the thickness of cell i in the z direction

II-3 Magnetic Field Dip Angle

For the simulation of the auroral cusp there was no need to take into account the angle between the earth's magnetic field lines and the vertical cells since this angle was essentially zero. That is to say, the diffusion and gravitational drift of O+ and H+ is parallel to the cells in the auroral cusp region. However, since it was decided to

simulate the mid-latitude ionosphere using initial profiles measured at Millstone Hill, the magnetic field dip angle had to be taken into account. This was because at Millstone Hill the geocentric dip angle is 72 deg and thus diffusion and gravitational drift would not take place along the same axis as the vertically stacked cells. Figure II-2 shows the geometry of the situation.

From Figure II-2 it is seen that:

$$V_{g,z} \sim g \sin^2 I$$

Where $V_{g,z}$ is the gravitational drift velocity in the z direction and

$$V_{D,z} = V_{D,h} \sin I$$

Where $V_{D,z}$ is the diffusion drift velocity in the z direction and $V_{D,h}$ is the diffusion drift velocity along the magnetic field line and I the geocentric dip angle of the magnetic field line.

Using the well known relation

$$V_{D,h} \sim D \frac{1}{N} \frac{dN}{dh}$$

FIGURE II-2

MAGNETIC FIELD DIP ANGLE

EFFECT ON PLASMA TRANSPORT

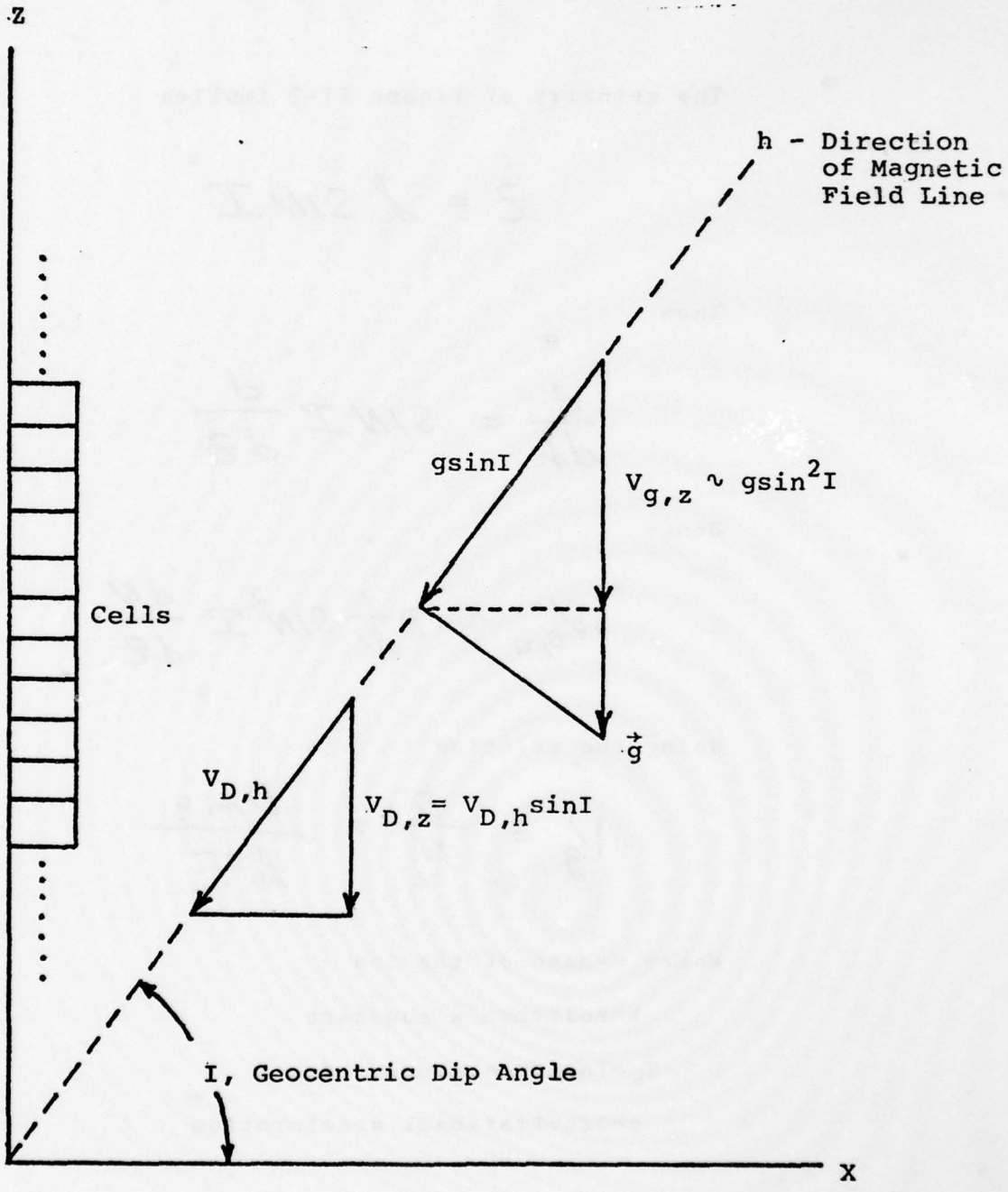

Where D= Diffusion coefficient

N=Number density of a species

The geometry of Figure II-2 implies

$$z = h \sin I$$

Thus

$$\frac{d}{dh} = \sin I \frac{d}{dz}$$

Hence

$$V_{D,z} \sim D \frac{1}{N} \sin^2 I \frac{dN}{dz}$$

Using the relation

$$V_g = \frac{D}{H_i} = \frac{Dmg}{kT_i}$$

Where m=Mass of the ion

k=Boltzman's constant

T_i=Ion temerature, deg K

g=Gravitational acceleration

Then

$$V_{g,z} = \frac{Dm}{kT_i} \sin^2 I \, g$$

And

$$V_{p,z} \sim V_{O,z} + V_{g,z}$$

$$V_{p,z} \sim D \sin^2 I \left[\frac{1}{N} \frac{dN}{dz} + \frac{m}{kT_i} g \right]$$

Where $V_{p,z}$ is the effective plasma velocity in the z direction. Conveniently, $D \sin^2 I$ can be regarded as an effective diffusion coefficient in the calculation of plasma transport due to diffusion and gravitational drift. This was done in the computer coding.

II-4 Neutral Atmosphere

The background neutral atmosphere of the model consisted of O, N2, O2, H and He. The atmosphere used was the 1000^{0} K thermopause model from Banks and Kockarts, (1973). The temperature profile of this model neutral atmosphere was also used. Neutral and ion temperatures were set equal to these model values. Electron temperature was set equal to twice the ion temperature.

II-5 Transport

The transport of plasma includes diffusion due to

concentration gradients and drift due to the gravitational field of the earth. The transport of O+ and H+ are handled in the same way so a single, general explanation may be used. Figure II-3 shows two representative cells and the relevant geometrical quantities.

Let

$D_{a,b}$ = The diffusion coefficient of species a through species b.

D_a = The overall diffusion coefficient for species a

$C_{a,i}$ = Ion concentration in cell i of species a

$N_{a,i}$ = Number of ions in cell i of species a

Δt = The calculation time step

$A_{i,i+1}$ = The cross sectional area of the boundary between cells i and i+1

$Z_{i,i+1}$ = The center to center distance between the cells i and i+1

L_i = The thickness of cell i

T_e = Electron temperature

T_i = Ion temperature

$C_{e,i}$ = Electron concentration in cell i

V_i = Volume of cell i

FIGURE II-3

PLASMA TRANSPORT

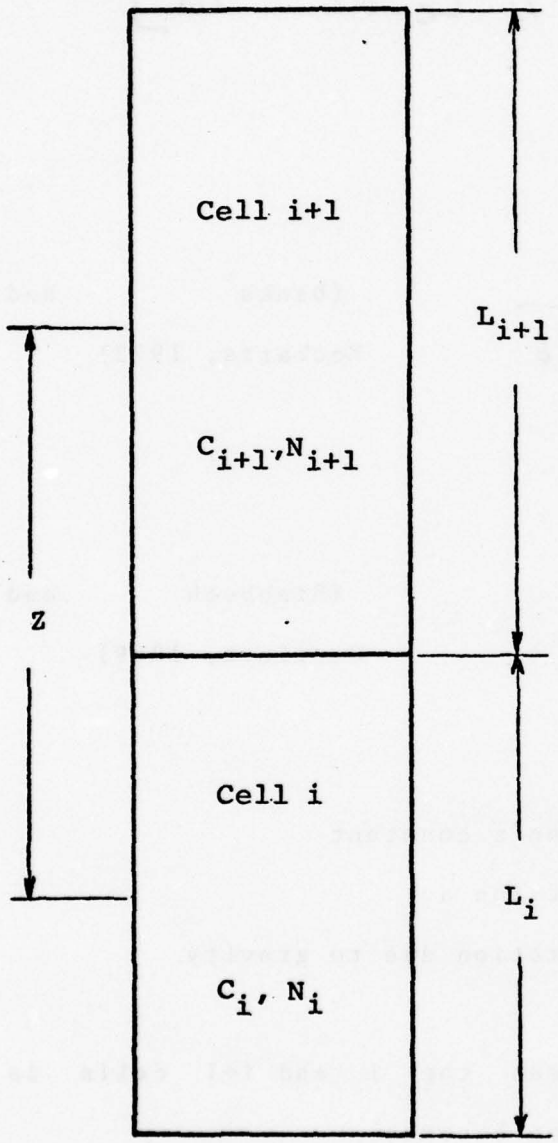

$$D_{i,i+1} = \frac{L_i D_i + L_{i+1} D_{i+1}}{L_i + L_{i+1}}$$

= Effective Diffusion Coefficient Between Cells i and i+1

The overall drift velocity, U_a, for an ion species a is given by (Banks and Holzer, 1969)

$$U_a = D_a\left[\frac{1}{C_{a,i}}\frac{\partial C_{a,i}}{\partial z} + \frac{T_e}{T_i}\frac{1}{C_e}\frac{\partial C_{e,i}}{\partial z} + \frac{1}{H_a}\right]$$

Where

$$\frac{1}{D_a} = \sum_{b\neq a}\frac{1}{D_{a,b}}$$ (Banks and Kockarts, 1973)

$$H_a = \frac{k\,T_a}{m_a\,g(z)}$$ (Rishbeth and Garriott, 1969)

$T_a = T_i$

k = Boltzman's constant

m_a = mass of ion a

$g(z)$ = acceleration due to gravity

When the boundary between the i and i+1 cells is considered in FES this equation becomes

$$U_{a,i\to i+1} = D_{a,i}\left[\frac{1}{C_{a,i}}\frac{C_{a,i+1}-C_{a,i}}{z_{i,i+1}} + \frac{T_e}{T_i}\frac{1}{C_{e,i}}\frac{C_{e,i+1}-C_{e,i}}{z_{i,i+1}} + \frac{1}{H_{a,i}}\right]$$

In practice, the diffusion coefficient $D_{a,i}$ is replaced by an effective diffusion coefficient, $D'_{a,i\to i+1}$, given by

$$D'_{a,i\to i+1} = SIN^2 I \left[\left(L_i D_{a,i} + L_{i+1} D_{a,i+1} \right) \Big/ \left(L_i + L_{i+1} \right) \right]$$

where the $SIN^2 I$ factor takes into account the geocentric dip angle I and the term in brackets weights $D_{a,i}$ and $D_{a,i+1}$, the diffusion coefficients within the cells, according to cell size.

The values $D_{a,b}$ used in the model for the diffusion of O+ and H+ were taken from Banks and Kockarts, (1973). The values are shown in Table II-1.

Plasma movement across the boundary between cell i and cell i+1 during a time step t is described by

$$\left.\begin{aligned}
\Delta N_{a,i} &= U_{a,i\to i+1} A_{i,i+1} C_{a,i} \Delta t \\
\Delta N_{a,i+1} &= -\Delta N_{a,i} \\
\Delta C_{a,i} &= \frac{\Delta N_{a,i}}{V_i} = U_{a,i\to i+1} C_{a,i} \Delta t \frac{A_{i,i+1}}{V_i} \\
\Delta C_{a,i+1} &= \frac{\Delta N_{a,i+1}}{V_{i+1}} = U_{a,i\to i+1} C_{a,i} \Delta t \frac{A_{i,i+1}}{V_{i+1}} \\
C_{a,i}(t+\Delta t) &= C_{a,i}(t) + \Delta C_{a,i} \\
C_{a,i+1}(t+\Delta t) &= C_{a,i+1}(t) + \Delta C_{a,i+1}
\end{aligned}\right\} \quad (II-1)$$

TABLE II-1
DIFFUSION COEFFICIENTS

$D_{H+ - O} = 3.71 \times 10^{16} \; T_{i/n(O)}$ CM^2/SEC

$D_{H+ - O_2} = 2.57 \times 10^{16} \; T_{i/n(O_2)}$

$D_{H+ - N_2} = 2.45 \times 10^{16} \; T_{i/n(N_2)}$

$D_{H+ - H_e} = 7.80 \times 10^{16} \; T_{i/n(H_e)}$

$D_{H+ - O+} = 6.88 \times 10^{7} \; (T_i)^{5/2}/n(O+)$

$D_{H+ - H} = 8.00 \times 10^{17} \; (T_i)^{\frac{1}{2}}/n(H)\,(1+T_n/T_i)^{\frac{1}{2}}$

$D_{O+ - O} = 3.10 \times 10^{17} \; (T_i)^{\frac{1}{2}}/n(O)\,(1+T_n/T_i)^{\frac{1}{2}}$

$D_{O+ - O_2} = 7.20 \times 10^{15} \; T_{i/n(O_2)}$

$D_{O+ - N_2} = 8.50 \times 10^{15} \; T_{i/n(N_2)}$

$D_{O+ - H_e} = 5.60 \times 10^{16} \; T_{i/n(H_e)}$

$D_{O+ - H} = 4.03 \times 10^{16} \; T_{i/n(H)}$

$D_{O+ - H+} = 9.39 \times 10^{7} \; (T_i)^{5/2}/n(H+)$

T_i = Ion Temperature

T_n = Neutral Temperature

Equations II-1 are of the form of equation I-1 which represented an update of a general parameter.

In this manner the transport of O+ and H+ across all relevant cell boundaries is calculated and the respective concentrations are updated after each time step.

II-6 Chemistry

Table II-2 lists the chemical reactions included in the model as well as the corresponding reaction rates. The rates used are from Banks and Kockarts, (1973). Since all the chemical reactions are handled in the same way a single general explanation will be given.

Let

A, B, C, D = The concentrations of four different species within a cell

k = The reaction rate of a given reaction

Δt = The calculation time step

Then for the chemical reaction

$$A + B \xrightarrow{k} C + D$$

TABLE II-2

CHEMICAL REACTIONS AND RATES

Reactions	Reaction Rates (cm^3/sec)
$O+ + N_2 \longrightarrow NO+ + N$	$k = 2 \times 10^{-12}$
$NO+ + e \longrightarrow N + O$	$k = 2 \times 10^{-7}$
$O+ + O_2 \longrightarrow O_2+ + O$	$k = 3.46 \times 10^{-10} / (T_n)^{\frac{1}{2}}$
$O_2+ + e \longrightarrow O + O$	$k = 2.81 \times 10^{-5} / (T_e)^{0.85}$
$O+ + H \longrightarrow O + H+$	$k = 2.5 \times 10^{-11} (T_n)^{\frac{1}{2}}$
$O + H+ \longrightarrow O+ + H$	$k = 2.3 \times 10^{-11} (T_i)^{\frac{1}{2}}$

T_e = Electron Temperature (Kelvin)

T_i = Ion Temperature

T_n = Neutral Temperature

The following relations hold

$$\Delta A = -k A B \Delta t$$

$$\Delta B = -k A B \Delta t$$

$$A(t+\Delta t) = A(t) + \Delta A$$

$$B(t+\Delta t) = B(t) + \Delta B$$

Here, again, is a physical process changing the concentrations of certain species . It is handled in the usual way, see eq. I-1. It may be that the concentrations of the products of the above reaction, namely C and D, are also of interest. In this case, by referring to the molar balanced chemical equation (not shown) the changes in the concentrations of the products C and D can be related very easily to the concentration changes ΔA or ΔB . This is possible since chemical reactions do not involve the transport of material between cells that may be of different sizes. Reactions take place within cells and therefore the volume is constant making the calculation of the change in the concentration of a product very straightforward.

II-7 Production of O+ ions

The production of O+ ions due to the precipitation of energetic electrons into the ionosphere was simulated by the computer model. This was accomplished by using an O+ production rate, due to precipitating electrons, calculated by Knudsen et al (1977).

A graph of this production function is shown in Figure II-4. This function is appropriate for the winter day cusp simulation of the auroral ionosphere, the results of which are presented in the next chapter.

The production function shown in Figure II-4 is given in units of number of O+ ions/cm**3-sec. In this form it is natural to handle O+ production in the model analogously to chemistry.

Let

P = Production rate of O+ ions (#/cm**3-sec)

Δt = Calculation time step

$[O^+]$ = Concentration of O+ ions

$[e]$ = Concentration of electrons

FIGURE II-4

DAYSIDE CUSP O+ PRODUCTION FUNCTION

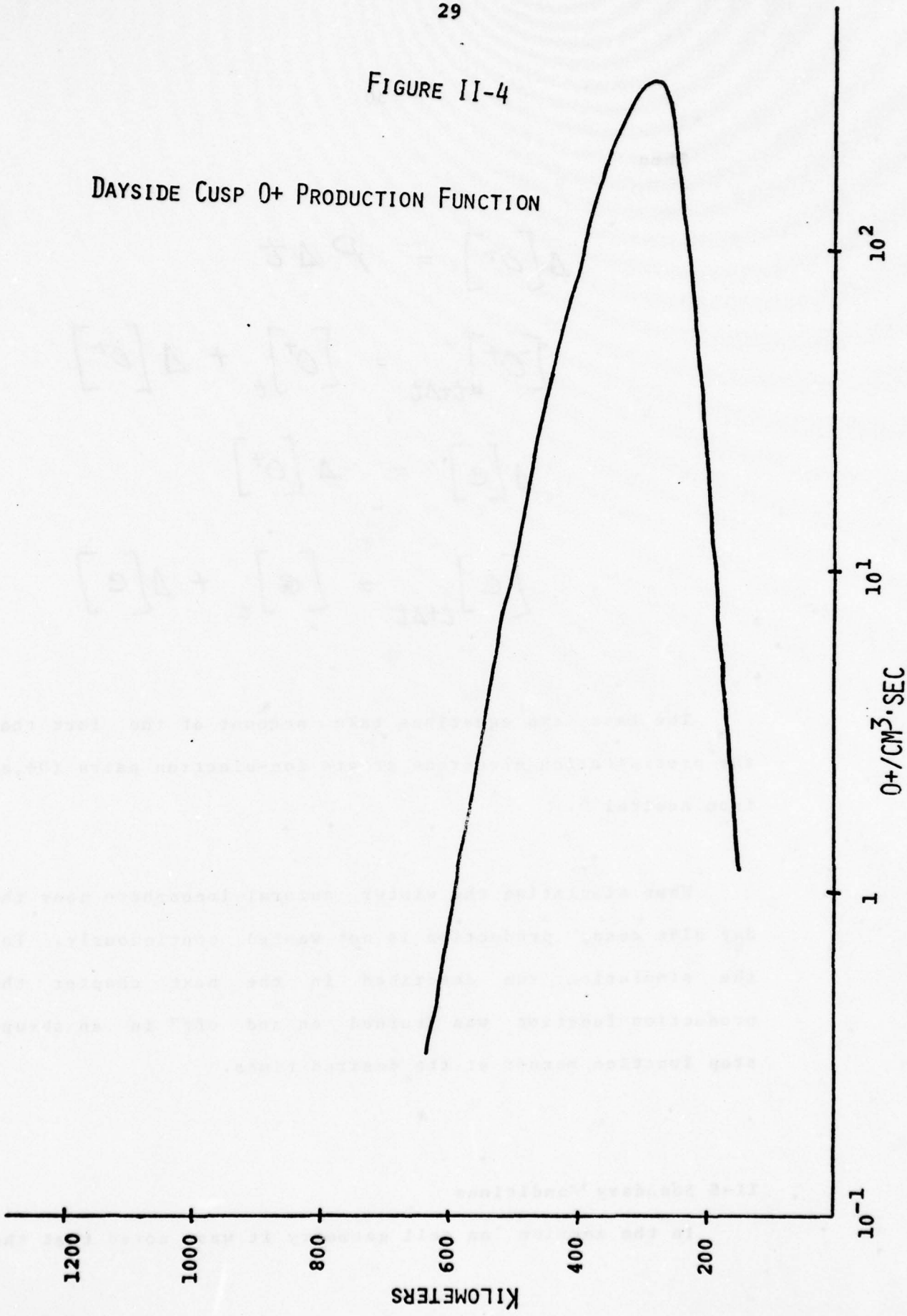

Then

$$\Delta[O^+] = P\,\Delta t$$

$$[O^+]_{t+\Delta t} = [O^+]_t + \Delta[O^+]$$

$$\Delta[e] = \Delta[O^+]$$

$$[e]_{t+\Delta t} = [e]_t + \Delta[e]$$

The last two equations take account of the fact that the precipitating electrons create ion-electron pairs (O+,e) from neutral O.

When simulating the winter auroral ionosphere near the day side cusp, production is not wanted continuously. For the simulation run described in the next chapter the production function was "turned on and off" in an abrupt step function manner at the desired times.

II-8 Boundary Conditions

In the section on cell geometry it was noted that the

bottom cell was at a center height of 150 km and the top one at 2010 km. The reason for this large range was to establish realistic boundary conditions. It would have been possible, in principle, to use a smaller range and impose a constant plasma flux at a given height as a boundary condition. But it was decided not to do this as a large range was needed anyway since measurements at the day side cusp were available up to 1400 km and the problem of deciding on a suitable boundary flux could be avoided as explained below.

The boundary condition at 150 km is handled in an implicit way by allowing the various physical processes (diffusion, chemistry, gravitational drift, and O+ production) to operate normally. The interaction of these processes establishes an equilibrium condition which very accurately mimics a lower F region profile. Thus, in the case of the lower boundary condition, there was no need to impose an ad hoc constraint; the aeronomic processes alone generated a realistic profile and this fact inspires confidence in the accuracy of the model in the lower F region.

There are two major differences between the bottomside and the topside that affect the boundary conditions. First, on the bottomside, the neutral atmosphere is very dense in

comparison to that of the topside. Thus, even though the plasma gradient is larger on the bottomside, the actual rate of plasma transfer is small due to the relatively small diffusion coefficient ($D \sim 1/N$ where D is the diffusion coefficient and N is the concentration of the background medium; $V_g \sim D/H_i$ where V_g is the gravitational drift velocity and H_i is the ion scale height).

The second reason is that on the bottomside the downward diffusing O+ reacts quickly with N2 and O2 to form NO+ and O2+. These molecular ions in turn dissociatively recombine with electrons, thus there is no build-up of O+ in the lower cells due to transport.

The case is different on the topside. The neutral atmosphere is very tenuous, consequently, the diffusion coefficients are large. Upward diffusion is therefore large. Since there is very little N2 and O2 to augment the effect of the "diffusive barrier" reaction $O+ + H \longrightarrow H+ + O$, there can be, in any model with a finite number of cells, a build up of O+ in the upper region.

The solution to the boundary condition problem was to use many cells. This alone was not enough, though, since the plasma tube being mimicked extends to the other hemishpere and that is a very different geometry from that being used.

What was done was to add cells so that the center of the top cell (100 km thick) reached 2010 km and to not allow plasma transport into or out of the top cell. The effect of this is to allow the chemical reaction $H + O^+ \rightleftharpoons H^+ + O$ to establish an equilibrium between the O^+ and H^+ concentrations and to allow the top cell to act as an infinite sink or source as far as plasma transport is concerned. This imitates the plasma tube in a satisfactory way in this model since the region of interest is below 1500 km (it is only at such heights and below that we have actual measurements with which to compare the results). By anchoring the ion concentrations in this way (the chemical equilibrium reached will not differ greatly from the initial concentrations) at a height of 2010 km it is considered that the extent to which this is an ad hoc constraint will have very little effect at heights of 1500 km and below.

II-9 Calculation Time Step

In the first chapter it was stated that to illustrate the selection of an appropriate time step the specific physical system must be taken into account. In this section the physics incorporated in the model will be used to make some common sense arguments to establish an upper limit on the time step.

First consider transport.

Let

C_i = concentration in cell i

$Z_{i,i+1}$ = distance between centers of cells i and i+1

$T_{e,i}$ = electron temperature in cell i

$T_{i,i}$ = ion temperature in cell i

$D_{i,i+1}$ = effective diffusion coefficient between cells i and i+1

H_i = scale height of the ion species at cell i

$A_{i,i+1}$ = cross sectional area of boundary between cells i and i+1

V_i = volume of cell i

Consider that in cell i at the beginning of a calculation time step there is an initial concentration of a given ion species. Cell i has boundary interfaces with cells i+1 and i-1 (see Figure II-3). Across those two boundaries there can be plasma transport as was described above. At the end of the time step, after the concentrations have been updated, physical reality requires that

$$C_i(t+\Delta t) \geq 0$$

The plasma velocities across the two cell boundaries are given by (Banks and Holzer, 1969)

$$U_{i,i+1} = D_{i,i+1}\left[\frac{1}{C_i}\frac{C_{i+1}-C_i}{Z_{i,i+1}} + \frac{T_{e,i}}{T_{i,i}}\frac{1}{C_{e,i}}\frac{C_{e,i+1}-C_{e,i}}{Z_{i,i+1}} + \frac{1}{H_i}\right]$$

$$U_{i,i-1} = D_{i,i-1}\left[\frac{1}{C_{i-1}}\frac{C_i-C_{i-1}}{Z_{i,i-1}} + \frac{T_{e,i-1}}{T_{i,i-1}}\frac{1}{C_{e,i-1}}\frac{C_{e,i}-C_{e,i-1}}{Z_{i,i-1}} + \frac{1}{H_{i-1}}\right]$$

The amount of plasma transport in time Δt is

$$\Delta N_{i,i+1} = U_{i,i+1} A_{i,i+1} C_i \Delta t$$

$$\Delta N_{i,i-1} = -U_{i,i-1} A_{i,i-1} C_{i-1} \Delta t$$

$$\Delta C_i = \left(\Delta N_{i,i+1} + \Delta N_{i,i-1}\right)/V_i$$

Then

$$C_i(t+\Delta t) = C_i(t) + \Delta C_i \geq 0 \qquad (II-2)$$

By substituting in for ΔC_i and working through the algebra, eq. II-2 can be shown to be equivalent to

$$\underbrace{\left[U_{i,i-1} A_{i,i-1}\frac{C_{i-1}}{C_i} - U_{i,i+1} A_{i,i+1}\right]\frac{\Delta t}{V_i}}_{\text{"XMOD"}} \leq 1 \qquad (II-3)$$

Following the terminology introduced by Balko and Mendillo (1977), it is convenient to define a characteristic parameter called "XMOD" for each physical process in the simulation. Each XMOD relates the time step to physical and/or chemical parameters that are involved in the process it represents.

The XMOD in eq. II-3 is the dimensionless parameter that typifies the transpoprt calculation. Since U depends on the prevailing physical conditions, and A and V are fixed by the cell geometry, XMOD, or Δt, is fixed by the initial conditions but may be subject to change as the simulation progresses (see below).

Thus eq. II-3, which is a consequence of straightforward physical reasoning, sets an upper limit on the only "elastic" parameter appearing in it, namely Δt, the calculation time step. This upper limit can be used as a starting point in determining a suitable Δt for a calculation. Before discussing how this is done, the XMOD for chemistry will be derived.

Let

C_i = Concentration of a species in cell i

$\{B_j\}$ = A set of n species with which C

reacts in cell i

Δt = Calculation time step

Assume that at time t:

$$C_i(t) > 0$$

Physical reality demands that:

$$C_i(t+\Delta t) \geq 0$$

Furthermore:

$$\Delta C_i = - C_i(t)\, \Delta t \sum_{j=1}^{m} k_j B_j$$

Therefore:

$$C_i(t+\Delta t) = C_i(t) + \Delta C_i$$

$$= C_i(t) - C_i(t) \Delta t \sum_{j=1}^{m} k_j B_j \geq 0 \quad (II-4)$$

Since by assumption:

$$C_i(t) > 0$$

Equation II-4 becomes:

$$1 - \Delta t \sum_{j=1}^{m} k_j B_j \geq 0$$

Or

$$\underbrace{\Delta t \sum_{j=1}^{m} k_j B_j}_{\text{"XMOD"}} \leq 1 \qquad (II-5)$$

And

$$\Delta t \leq \frac{1}{\sum_{j=1}^{m} k_j B_j}$$

Equation II-5 defines XMOD for a chemical species in cell i which reacts with a set of chemical species $\{B_j\}$ with the reaction rates $\{k_j\}$.

It is not necessary to do an XMOD analysis for the other physical process in the model, namely production of O+ due to electron precipitation, since that process can only add plasma and therefore can never create a physically unrealistic condition such as a negative concentration.

The Δt must satisfy the XMOD criteria for transport and chemistry. Naturally the smaller of the two Δt's must be chosen. In this way a first estimate of an appropriate Δt is made. In practice it has been found that an XMOD as

large as 0.1 yields a time step that gives good results. This has been checked by taking a time step considerably smaller and running a calculation. It has been found that the much finer time step does not produce results significantly different from the "coarser" time step based on all XMODs being 0.1 or less.

It must be emphasized that XMOD may be a function of time and altitude. In the case of plasma transport, XMOD is a function of the diffusion coefficient whch is a function of the species concentrations. In the case of chemistry, XMOD is a direct function of species concentrations. Species concentrations are a function of both time and altitude.

Another point regarding XMOD must be emphasized. Each of the Xmods was derived independently of the others; i.e., each derivation assumed that only one process was acting and therefore that only one process was affecting the concentration of a particular species. This is obviously not the true picture in the ionosphere or in the one dimensional model. For example, in the one dimensional model O+ is subject to the processes of transport and four chemical reactions simultaneously. Consequently, a time step that satisfies each XMOD individually must be used judiciously. If the calculation were set up in such a way

that satisfies each XMOD individually must be used judiciously. If the calculation were set up in such a way that all the concentrations were updated at the end of each time step after all physical processes had operated, then the time step which satisfied the most stringent individual XMOD might not be sufficiently small to avoid instability in the calculation. This is because, in this case, an "aggregate" XMOD (an XMOD calculated taking into account the simultaneous action of several physical processes) would be needed to establish a suitable time step. What is done instead is to update the concentrations after each physical process operates. This has two advantages. First, it assures the usefulness and validity of the individual XMODs as indicators of calculation stability and second, it enables the use of different time steps for different processes. This potentially saves computer time if several processes have substantially different time steps based on individual XMODs. Recall that in the former scheme all processes would have to be calculated at the smallest time step required by any one of the individual processes. More will be said later on the use of multiple time steps.

When XMOD is used as a guide for checking the appropriateness of the length of the time step it must be calculated for all processes in all cells. This may be done periodically as the simulation progresses.

XMOD has been found in practice to be a reliable indicator of when a calculation is becomming critically near overshoot; usually manifested by creating a negative concentration. This experience has been gained not only with the one dimensional model described here, but also with a two dimensional model used to simulate the making of "ionospheric holes" (Balko and Mendillo, 1977).

II-10 Multiple Time Steps

It should be pointed out that a simulation need not use only one time step. In fact the one dimensional model described here uses five. The five time steps are for chemistry, O+ transpoprt in the lower zone, O+ transport in the upper zone, H+ transport in the lower zone, and H+ transport in the upper zone. The reference to upper and lower zones means that a different time step (i.e., a longer time step) was used at lower altitudes for the transport of H+ and O+ than at the higher altitudes, since at the lower altitudes the processes of diffusion and gravitational drift are much slower owing to the dense neutral atmosphere. The same time step was used for chemistry at all heights since the computer time required to calculate chemistry was quite small in comparison to transport, and the amount of real savings was not worth the added complexity.

The reason for using multiple time steps, of course, is to save computer time. There is no point in an FES calculation in using a very "fine" time step for any process at any spatial location when the overall accuracy of the results is determined by the process with the "coarsest" time step (by that is meant a time step that just barely meets the criterion imposed on it by the process's XMOD). The only complication introduced by using multiple time steps is that extra computer coding must be written to make sure that all processes at all spatial locations evolve together in synchronism.

The ultimate check on whether a set of time steps is suitable is to run the program with time steps that are much shorter than required based on XMODs, and then to run it with as large time steps as possible (still consistent with XMODs). This comparison run need only be for a short time, certainly not the entire simulation. If it is found that the two runs are in good agreement then the longer time steps are justified. This approach is based on the assumed accuracy of the run with the very short time steps. Given the algebraic form of the XMODs (which are a good indication of the sensitivity of the calculation to the size of the time step) it is clear that in every case decreasing the time step can have only a beneficial effect. This procedure merely determines the point at which the law of diminishing

returns sets in and enables the selection of the largest feasible time steps and thus minimizes computer time.

In the simulations done in this study the time steps used were of the order of one to two seconds.

II-11 Accuracy

All numerical schemes including FES are, of course, subject to the errors that may be present in the physics that is put into the model (for example diffusion coefficients, reaction rates and formulae that may be only approximately correct). And all numerical techniques are subject to the errors introduced by the finite word length of the computer used. FES has the advantage , though, of not being subject to another source of error that besets many numerical techniques and that is the errors inherent in the algorithms used. Recall that these techniques are explicitly concerned with solving a system of differential equations. In order to achieve that end approximations are often made in designing the technique in the first place. FES, being a straightforward simulation, is immune from such errors. There is no mathematical algorithm introducing error that must be taken into account. The only numerical source of error in the FES technique is due to the finite computer word size.

However, just as with other numerical techniques, the estimation of these errors is very difficult to make. The best way to minimize error with FES is to keep a careful watch on the XMODs and to directly check the suitability of the time steps by the comparison method.

Another procedure that proved useful in assuring the accuracy and stability of the calculation was to priodically check, as the simulation progressed, to see that in one time iteration the percent change of each of the species concentrations was not more than a couple of percent. This proved to be a very good test. If the percent change for any important species became too large, a judgement was made as to whether to decrease Δt.

II-12 Computer Code

The one dimensional model was written in Fortran for use on Boston University's IBM 370 computer. It was divided into a main program and several subroutines. A substantial amount of input data is needed to establish the cell geometry, the neutral atmosphere, the initial ionosphere and the O+ production function. Figure II-5 shows a functional block diagram of the computer code.

When the program is run the main program first reads in

FIGURE II-5

COMPUTER MODEL FLOW CHART

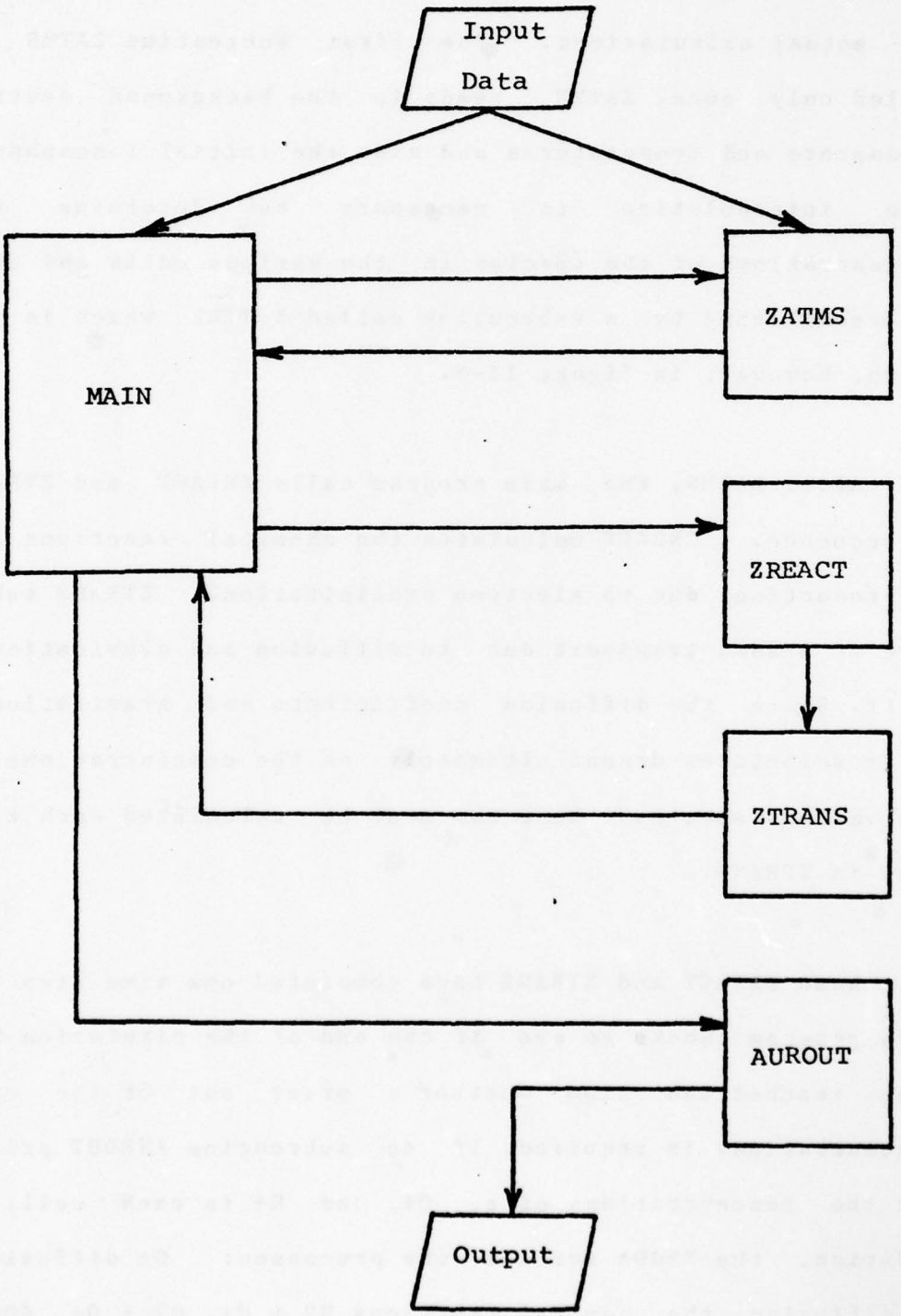

some control data and the cell geometry. From then on it functions merely to call various subroutines which perform the actual calculations. The first subroutine ZATMS is called only once. ZATMS reads in the background neutral atmosphere and temperatures and also the initial ionosphere. Some interpolation is necessary to determine the concentrations of the species in the various cells and this is accomplished by a subroutine called INTERP which is not shown, however, in Figure II-5.

After ZATMS, the main program calls ZREACT and ZTRANS in sequence. ZREACT calculates the chemical reactions and O+ production due to electron precipitation. ZTRANS takes care of plasma transport due to diffusion and gravitational drift. Since the diffusion coefficients and gravitational drift velocities depend ultimately on the concentrations of the various species these too must be calculated each time step in ZTRANS.

When ZREACT and ZTRANS have completed one time step the main program checks to see if the end of the simulation has been reached and also whether a print out of the cell concentrations is required. If so subroutine AUROUT prints out the concentrations of e, O+, and H+ in each cell. In addition, the XMODs for all the processes: O+ diffusion, H+ diffusion, the chemical reactions N2 + O+, O2 + O+, NO+ +

e, O_2^+ + e, O^+ + H, and O + H^+ are calculated and printed out. Also printed out are the percent changes in the species concentrations during the last time step before the printout. Recall that it is important to monitor the XMODs and percent changes to assure that the calculation does not become unstable.

When the end of the simulation is reached a final print out of the parameters is made by AUROUT and the program stops.

Chapter III

Dayside Auroral Cusp Simulation

III-1 Initial Profile

The initial electron profile used in the winter dayside cusp simulation was an average topside vertical electron density profile based on December 1971 data from the Isis 2 topside sounder. The actual profile was an average obtained at 75.5° Corrected Geomagnetic Latitude (Chacko and Mendillo, 1977). This profile is shown in Figure III-1.

The 75.5° CGL profile is an electron density profile. In order to use the ionospheric model an O+ and an H+ profile were needed. It would have been possible to assume an initial H+ profile of zero at all heights but that was considered unrealistic. Instead, the electron density profile just above the peak was considered to be equal to an O+ profile. A constant O+ scale height was defined and used to determine O+ at all other topside heights. The H+ profile was then calculated by subtracting the O+ profile from the electron profile. Thus the assumption was made that only two ion species existed at t=0, O+ and H+ (NO+ and O2+ profiles were zero at all heights at t=0).

III-2 O+ Production Function

The purpose of this simulation was to mimic the

FIGURE III-1

DAYSIDE CUSP PROFILE, T=0

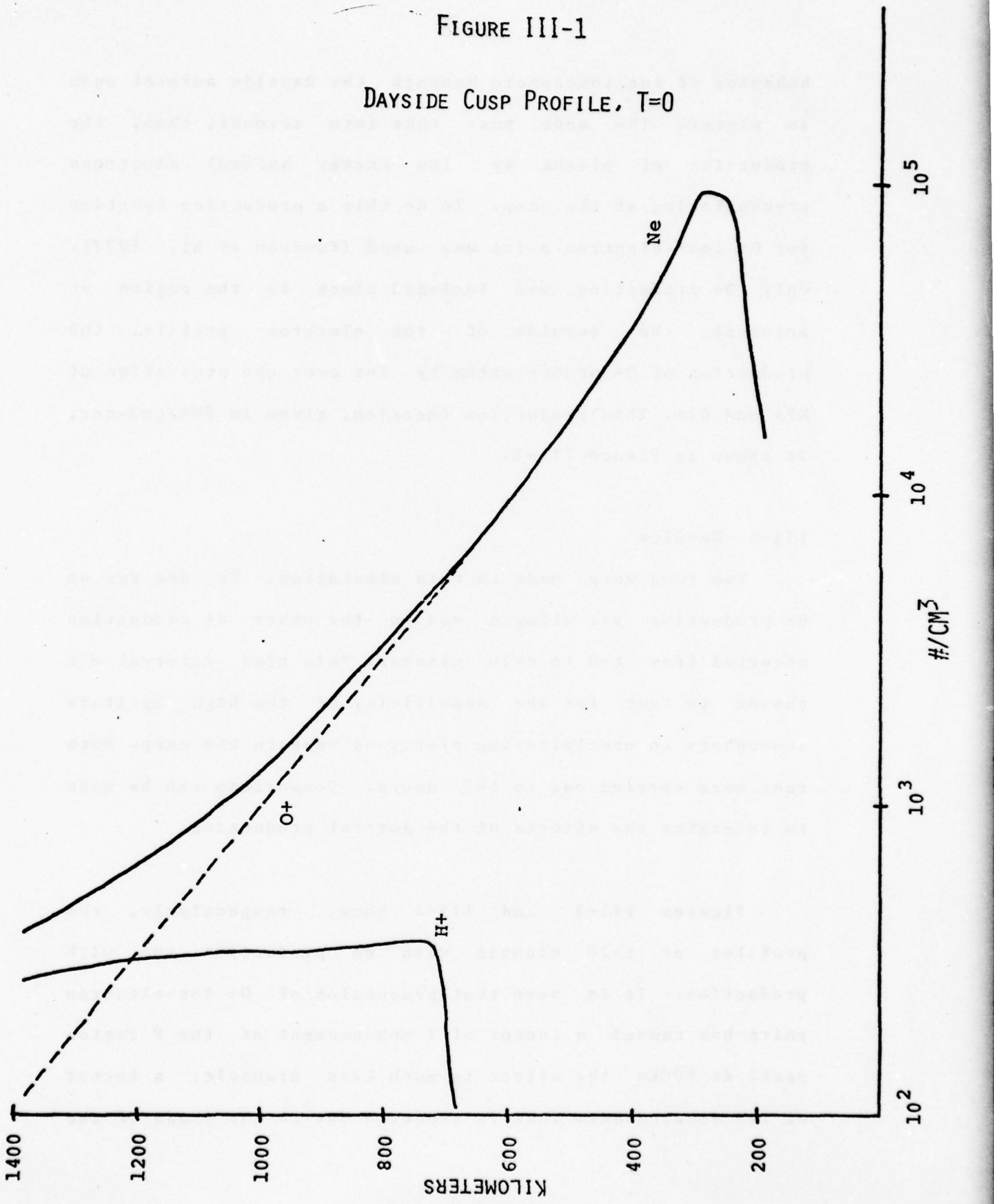

behavior of the ionosphere beneath the dayside auroral cusp in winter. The model must take into account, then, the production of plasma by low energy auroral electrons precipitating at the cusp. To do this a production function for O+ ion- electron pairs was used (Knudsen et al, 1977). Only O+ production was included since in the region of interest, the topside of the electron profile, the production of O+ predominates by far over the production of N2+ and O2+. This production function, given in #O+/cm3-sec, is shown in Figure III-2.

III-3 Results

Two runs were made in this simulation. In one run no O+ production was allowed and in the other O+ production occurred from t=0 to t=20 minutes. This time interval was chosen to test for the sensitivity of the high latitude ionosphere to precipitating electrons beneath the cusp. Both runs were carried out to t=2 hours. Comparison can be made to determine the effects of the auroral production.

Figures III-3 and III-4 show, respectively, the profiles at t=20 minutes with no production and with production. It is seen that production of O+ ion-electron pairs has caused a factor of 7 enhancement at the F region peak. At 800km the effect is much less dramatic; a factor of 1.3 enhancement. This is expected due to the shape of the

FIGURE III-2

DAYSIDE CUSP O+ PRODUCTION FUNCTION

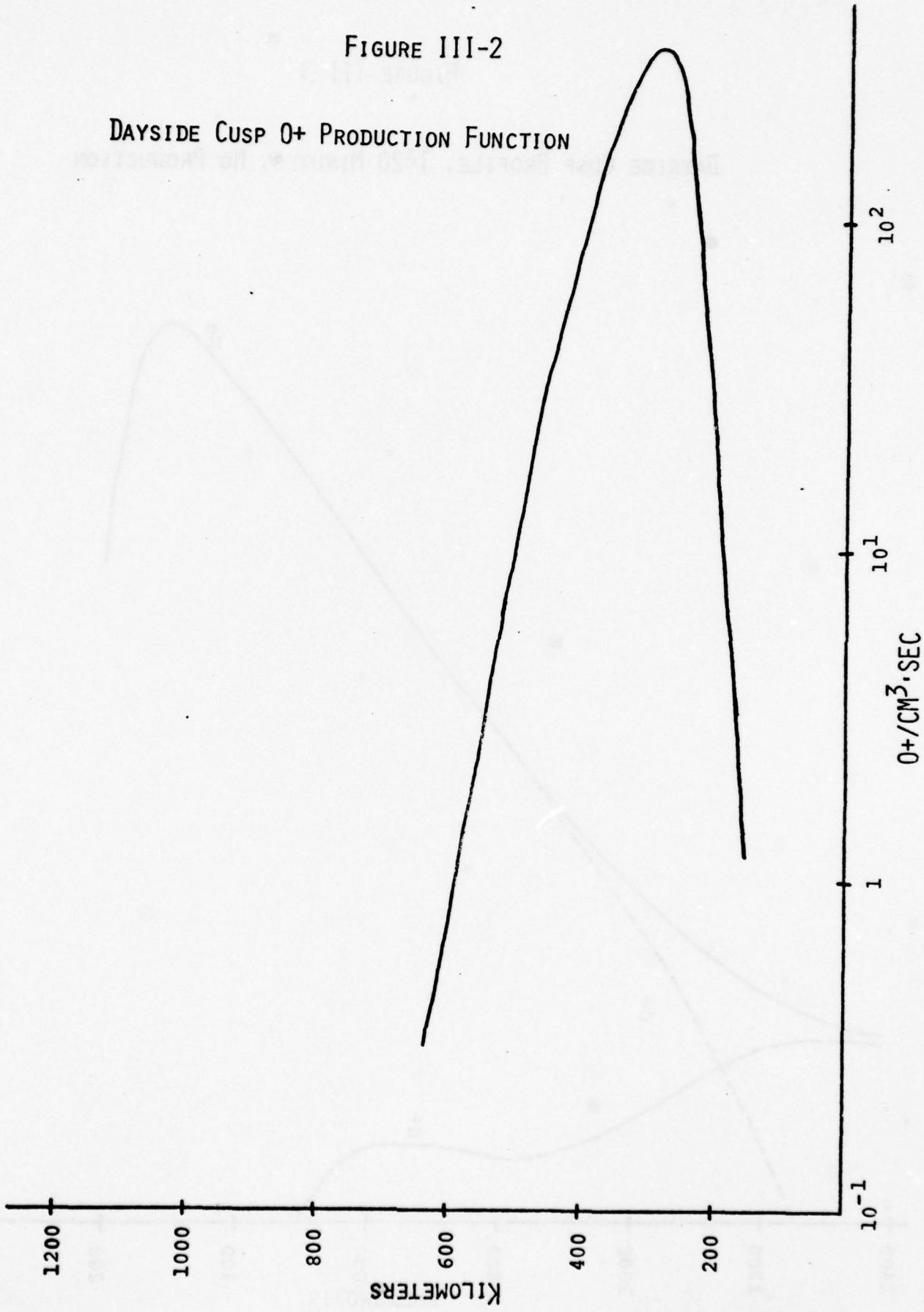

FIGURE III-3

DAYSIDE CUSP PROFILE, T=20 MINUTES, NO PRODUCTION

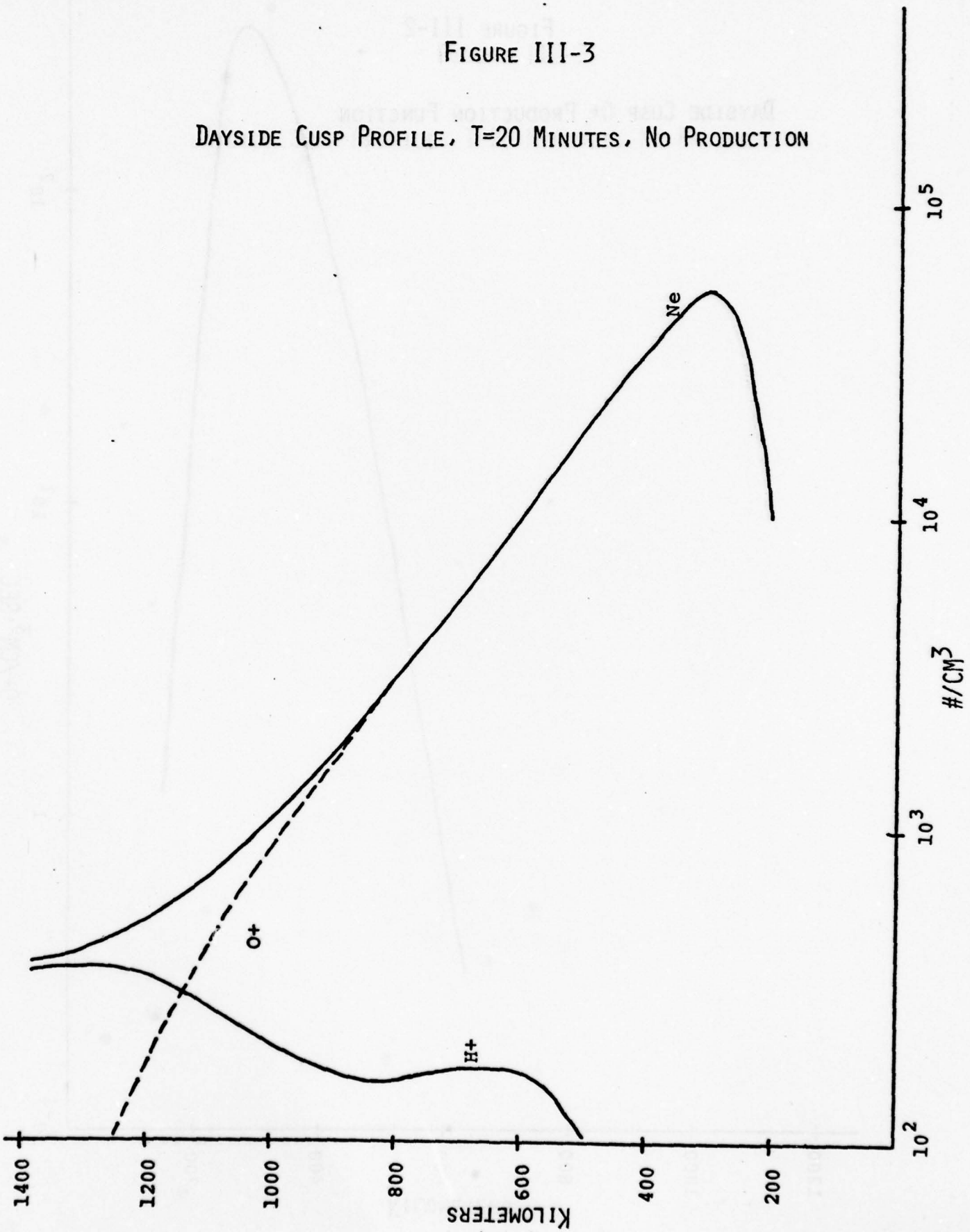

FIGURE III-4

DAYSIDE CUSP PROFILE, T=20 MINUTES
PRODUCTION T=0 TO T=20 MINUTES

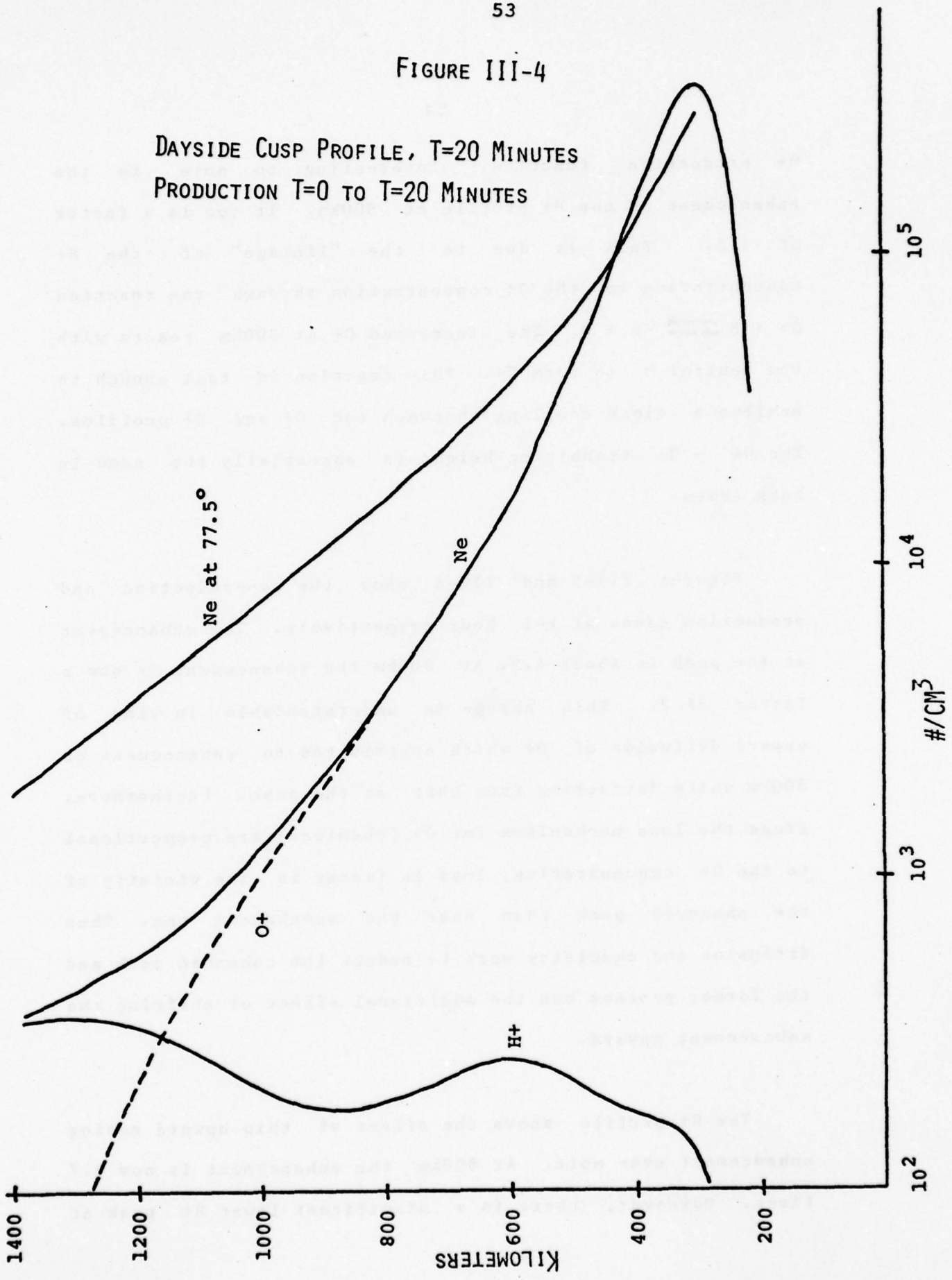

O+ production function. Interesting to note is the enhancement of the H+ profile at 800km. It too is a factor of 1.3. This is due to the "linkage" of the H+ concentration to the O+ concentration through the reaction $O^+ + H \rightleftharpoons H^+ + O$. The increased O+ at 800km reacts with the neutral H to form H+. This reaction is fast enough to achieve a close coupling between the O+ and H+ profiles. The O+ - H+ transition height is essentially the same in both cases.

Figures III-5 and III-6 show the no-production and production cases at t=1 hour respectively. The enhancement at the peak is about 4.5. At 800km the enhancement is now a factor of 2. This change is understandable in view of upward diffusion of O+ which contributes to enhancement at 800km while detracting from that at the peak. Furthermore, since the loss mechanisms for O+ (chemical) are proportional to the O+ concentration, loss is faster in the vicinity of the enhanced peak than near the unenhanced one. Thus diffusion and chemistry work to reduce the enhanced peak and the former process has the additional effect of shifting the enhancement upward.

The H+ profile shows the effect of this upward moving enhancement even more. At 800km the enhancement is now 2.7 times. Moreover, there is a significant lower H+ peak at

FIGURE III-5

DAYSIDE CUSP PROFILE, T=1 HOUR, NO PRODUCTION

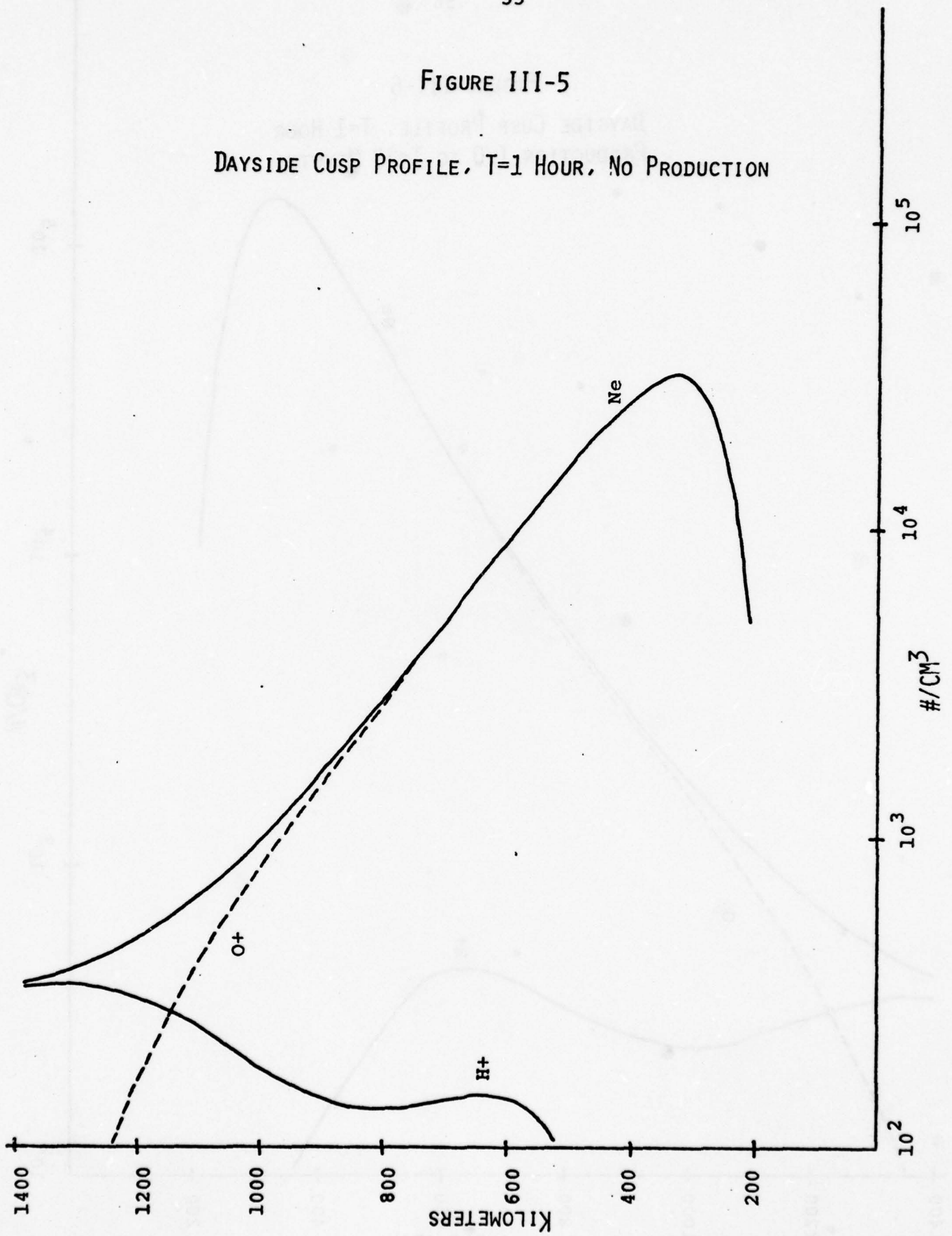

FIGURE III-6

DAYSIDE CUSP PROFILE, T=1 HOUR
PRODUCTION T=0 TO T=20 MINUTES

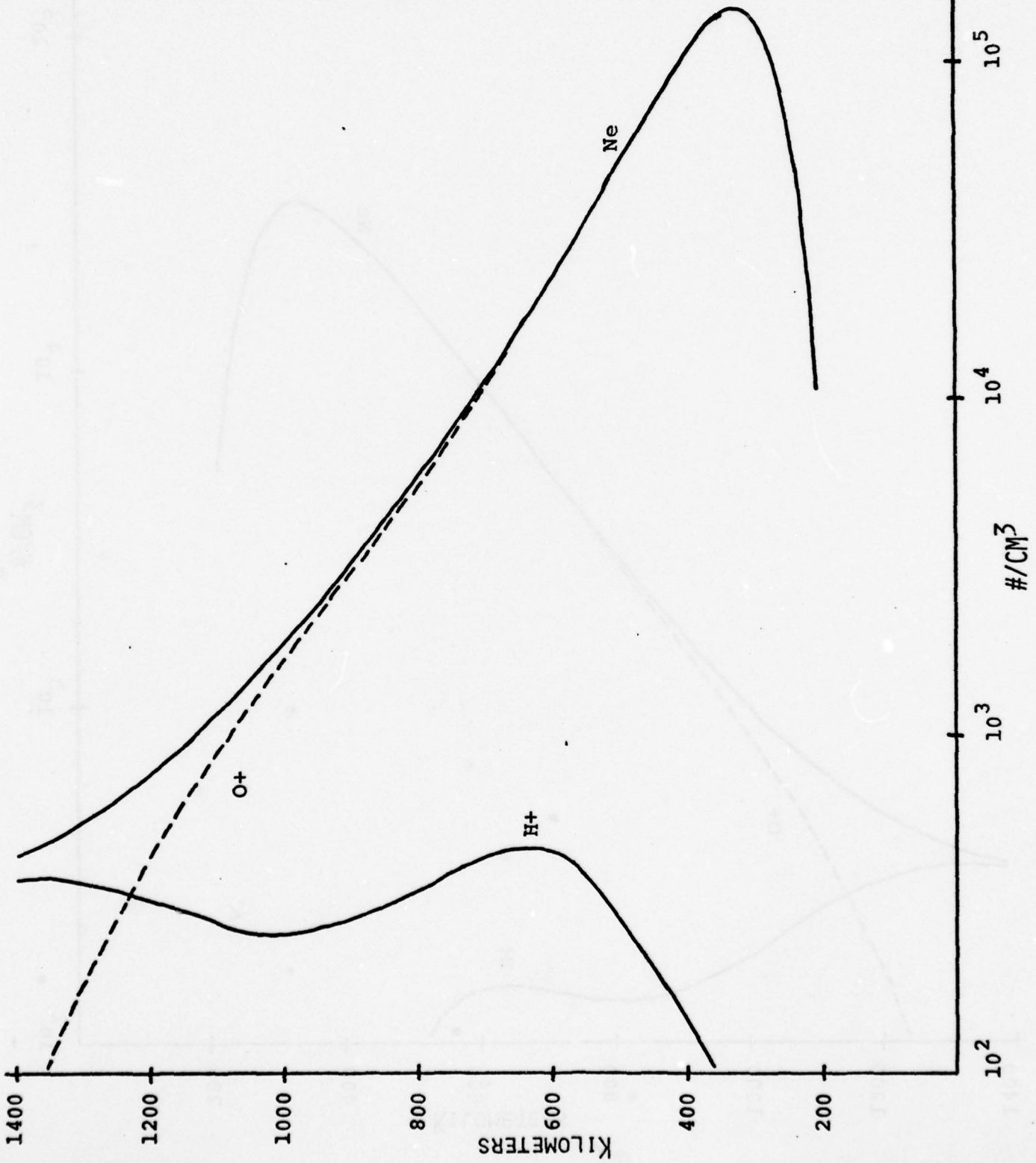

about 640km. This is also evident in the no production case shown in Figure III-5. The enhancement factor at this lower H+ peak is 3. The H+ profile, as mentioned above, is closely coupled to the O+ profile by chemistry and this makes it a sensitive indicator of upward movement of O+ enhancement due to diffusion.

The O+ - H+ transition height now shows a substantial difference between the two cases. Originally, at t=0, the transition height was at 1200km. Now at t=1 hour in the no production case, the transition height has moved downward to 1140km and in the case with production it has moved upward to 1240km. This effect can be understood in terms of the upward diffusion of O+ dominating over loss (pushing up the transition height) and, in the case without production, the loss of O+ at the higher altitudes due primarily to downward transport which helps to maintain the F region profile shape during the night.

Figures III-7 and III-8 show, respectively, the profiles without production and with production at t=2 hours. The F region peak enhancement has further declined to 3.4 times. At 800km the enhancement has further increased to 3.4 times as the upward diffusion of O+ produced at lower altitudes continues. The lower H+ peak persists and has moved upward toward 700km. The O+ - H+

FIGURE III-7

DAYSIDE CUSP PROFILE, T=2 HOURS, NO PRODUCTION

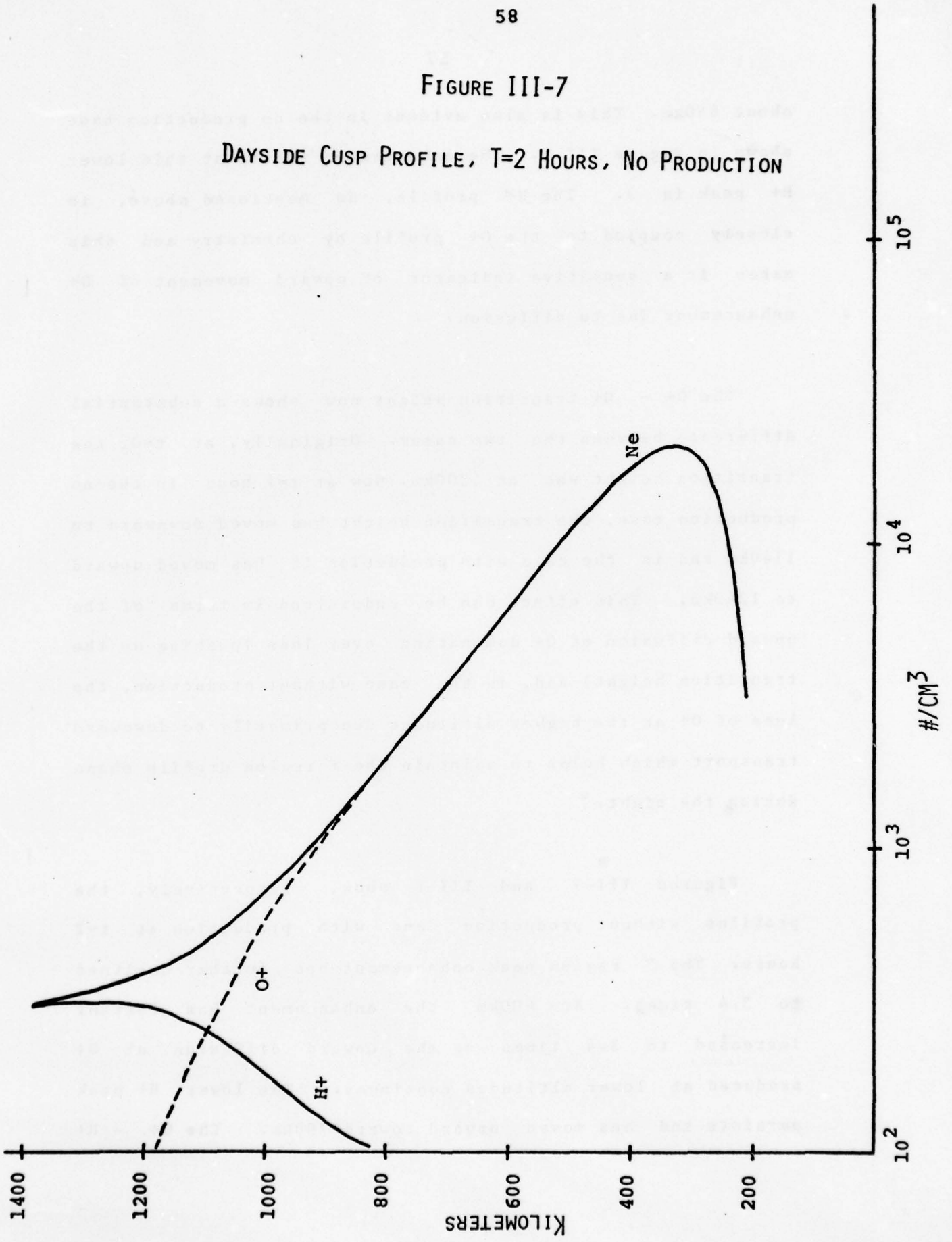

FIGURE III-8

DAYSIDE CUSP PROFILE, T=2 HOURS

PRODUCTION T=0 TO T=20 MINUTES

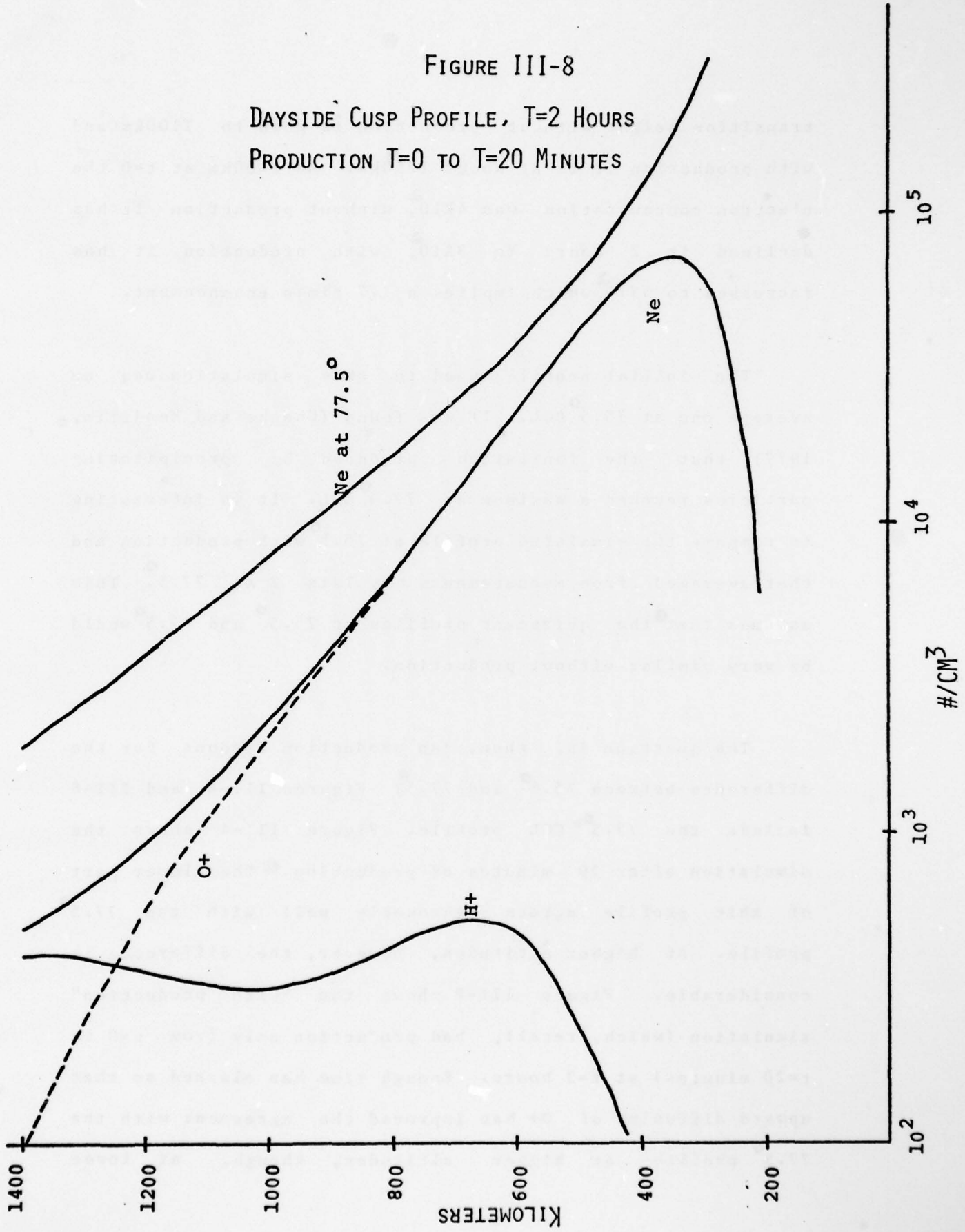

transition height without production is down to 1100km and with production it is at about 1250km. At 1400km at t=0 the electron concentration was $4X10^2$, without production it has declined in 2 hours to $3X10^2$, with production it has increased to $5X10^2$ which implies a 1.7 times enhancement.

The initial profile used in this simulation was an average one at 75.5° CGL. It was found (Chacko and Mendillo, 1977) that the ionization produced by precipitating particles reached a maximum at 77.5° CGL. It is interesting to compare the simulated profile at 75.5° with production and that averaged from measurements by Isis 2 at 77.5°. This assumes that the quiescent profiles at 75.5° and 77.5° would be very similar without production.

The question is, then, can production account for the difference between 75.5° and 77.5°? Figures III-4 and III-8 include the 77.5° CGL profile. Figure III-4 shows the simulation after 20 minutes of production. The lower part of this profile agrees reasonably well with the 77.5° profile. At higher altitudes, however, the difference is considerable. Figure III-8 shows the "with production" simulation (which, recall, had production only from t=0 to t=20 minutes) at t=2 hours. Enough time has elapsed so that upward diffusion of O+ has improved the agreement with the 77.5° profile at higher altitudes, though, at lower

altitudes, the agreement has worsened. The slope of the simulated profile matches the 77.5° profile well at 2 hours. If, instead of only one 20 minute burst of precipitating electrons, longer "exposure time" to cusp precipitations were used, much better agreement with the "steady-state" 77.5° CGL profile might be obtained. It is clear that this model could be used in such a detailed study.

Chapter IV

Night-Time Mid-Latitude Ionosphere Simulations

IV-1 Introduction

In the previous chapter the usefulness of the FES technique was demonstrated by the one dimensional model of the auroral ionosphere. In order to demonstrate the flexibility of FES it was decided to apply the one dimensional model to the mid-latitude ionosphere. This could be accomplished with minor changes; principle among them was the inclusion of the geomagnetic dip angle. Two different initial profiles were used, both from Millstone Hill (Evans and Holt,1977). They differ from the initial profile used in the cusp simulation in that, for each, the H+ - O+ transition height was 800km rather than 1200km. Both profiles are described below.

IV-2 December 6, 1972 Millstone Hill Profile

Figure IV-1 shows the December 6, 1972 Millstone Hill profile (Evans and Holt, 1977). It was selected to be used as a starting point for a night-time mid-latitude simulation principally because of its rather low O+ - H+ transition height. The question to be investigated was whether such a low transition height profile would remain stable during simulation with the one dimensional model. The O+ vertical velocity measurements for this profile made with the

FIGURE IV-1

MILLSTONE HILL PROFILE, DEC. 6, 1972

T=0

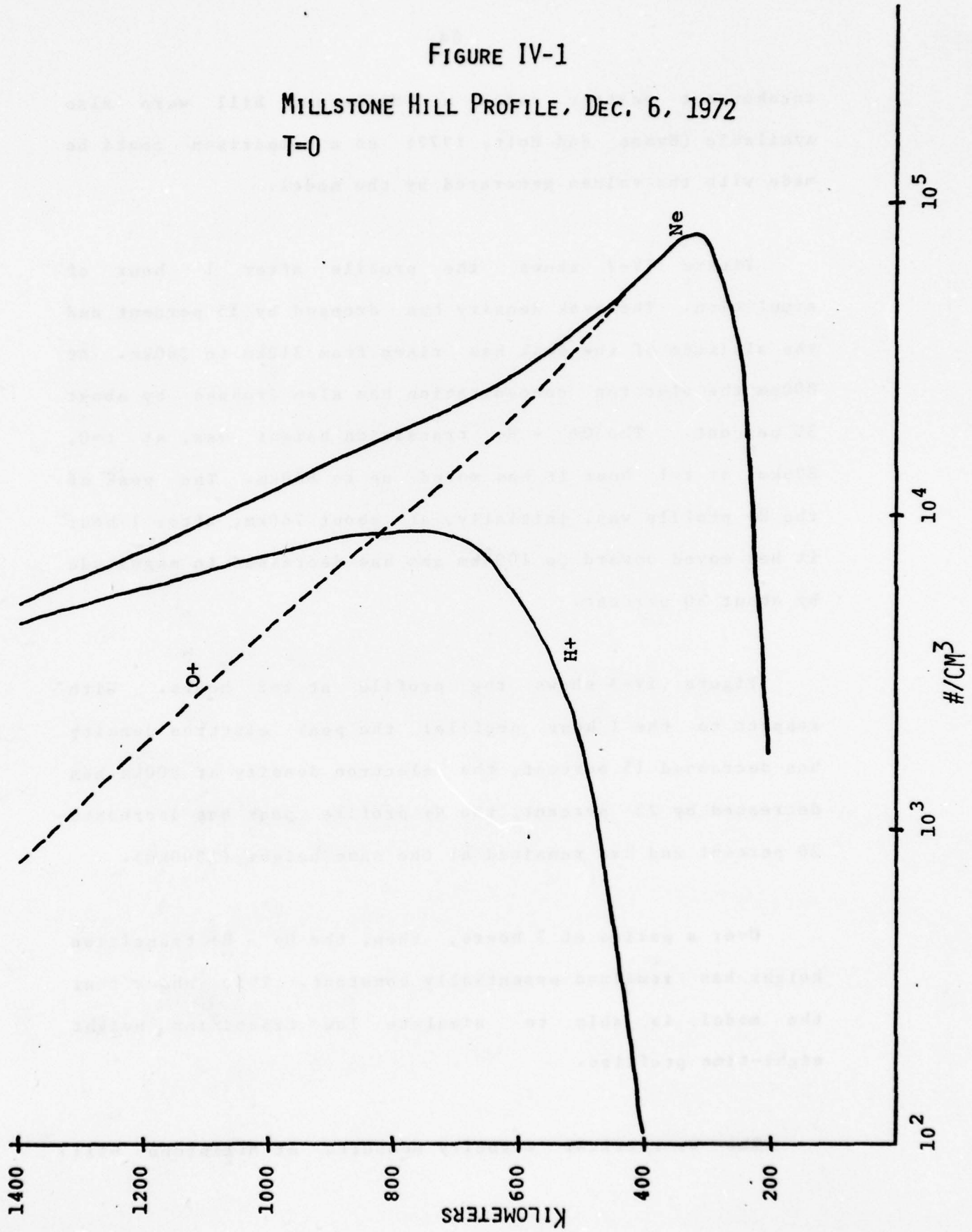

incoherrent scatter radar at Millstone Hill were also available (Evans and Holt, 1977) so a comparison could be made with the values generated by the model.

Figure IV-2 shows the profile after 1 hour of simulation. The peak density has dropped by 35 percent and the altitude of the peak has risen from 310km to 360km. At 800km the electron concentration has also dropped by about 35 percent. The O+ - H+ transition height was, at t=0, 820km, at t=1 hour it has moved up to 840km. The peak of the H+ profile was, initially, at about 740km, after 1 hour it has moved upward to 1000km and has decreased in magnitude by about 30 percent.

Figure IV-3 shows the profile at t=2 hours. With respect to the 1 hour profile: the peak electron density has decreased 15 percent, the electron density at 800km has decreased by 25 percent, the H+ profile peak has decreased 20 percent and has remained at the same height (1000km).

Over a period of 2 hours, then, the O+ - H+ transition height has remained essentially constant. This shows that the model is able to simulate low transition height night-time profiles.

The O+ vertical velocity measured at Millstone Hill

FIGURE IV-2

MILLSTONE HILL PROFILE, DEC. 6, 1972
T=1 HOUR

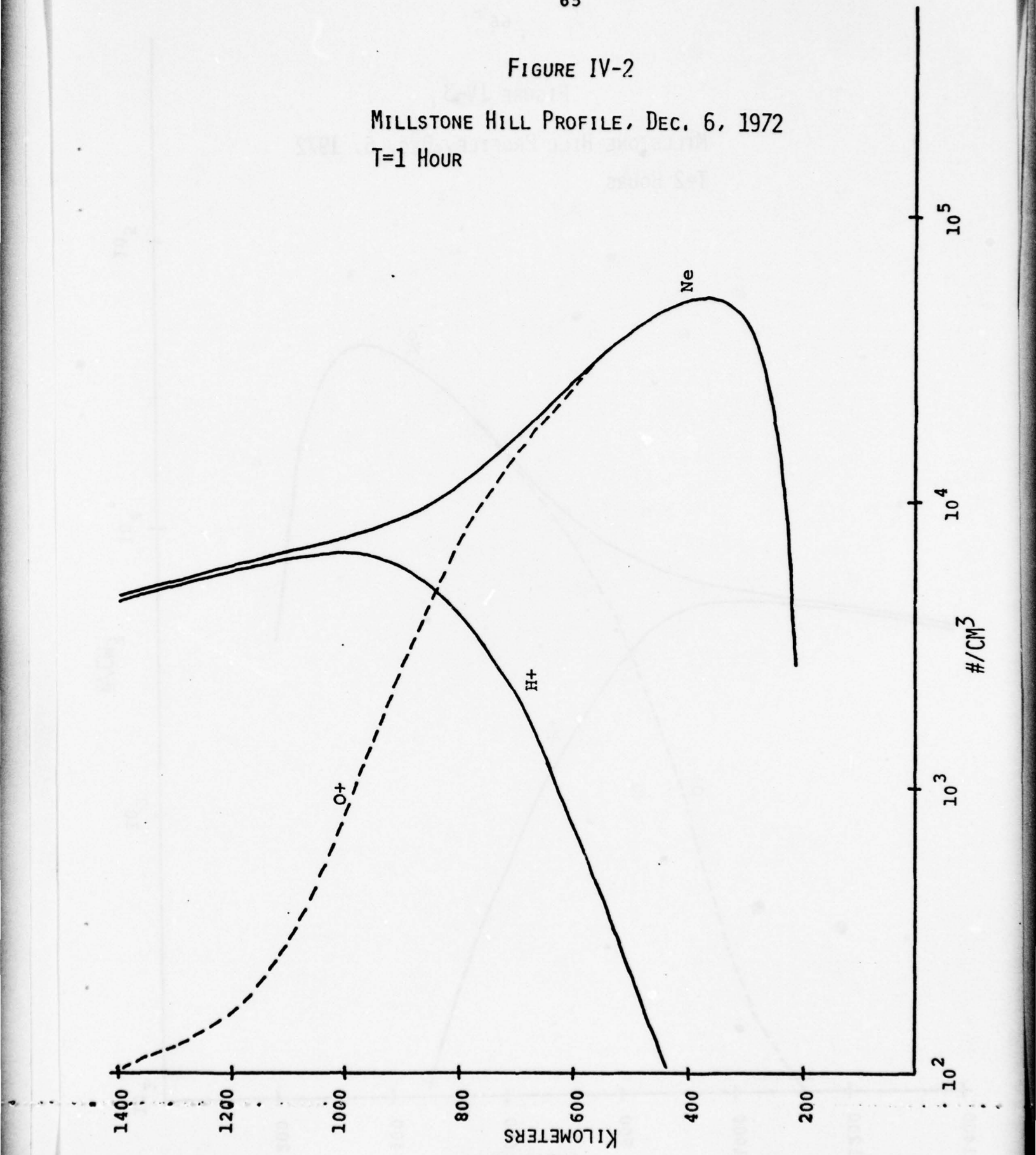

FIGURE IV-3

MILLSTONE HILL PROFILE, DEC. 6, 1972

T=2 HOURS

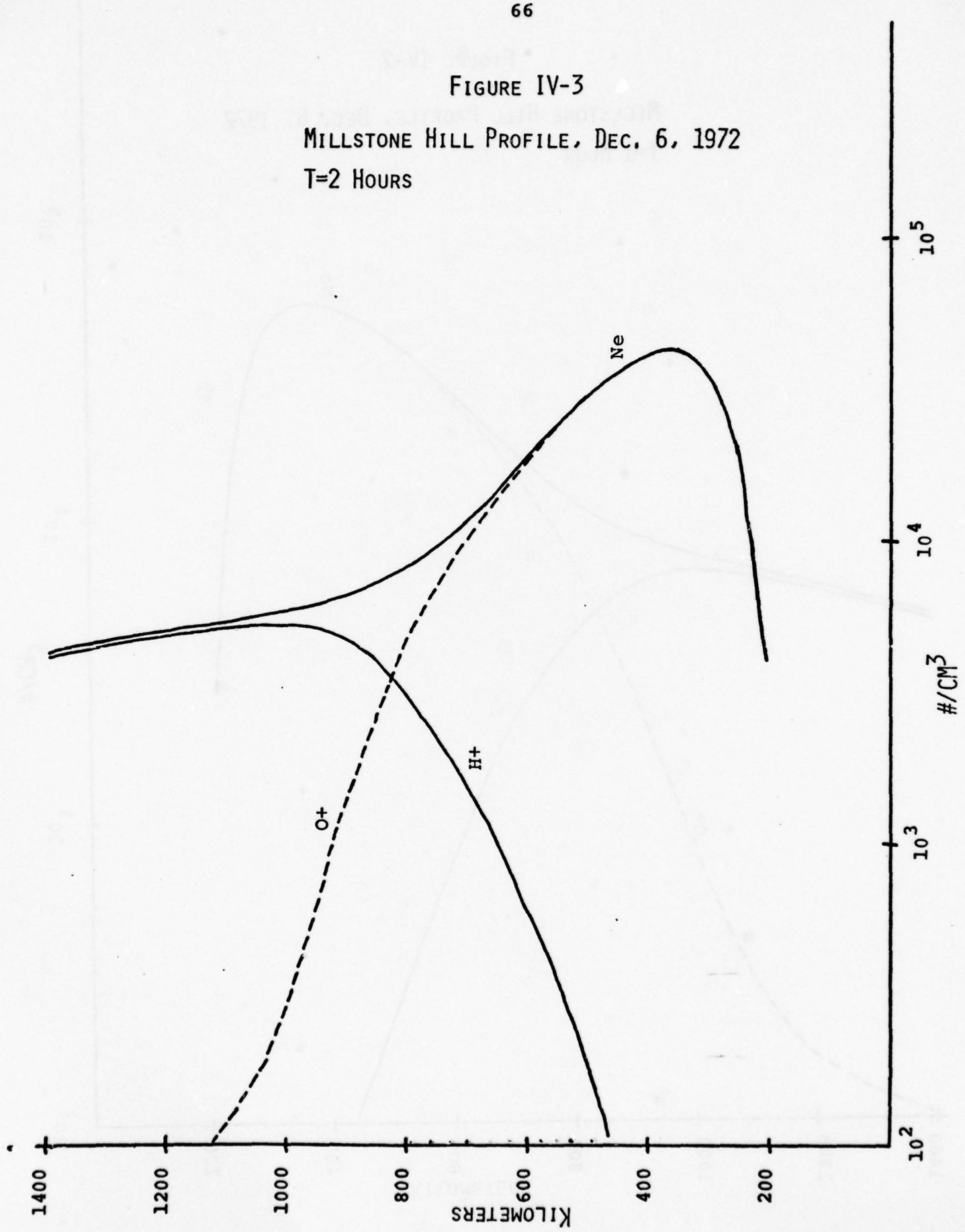

(Evans and Holt, 1977) at 300km, 525km, and 600km were -2000cm/sec (negative sign means toward the earth), -4800cm/sec and -7500cm/sec respectively. The values calculated during the simulation were, at the same heights respectively, -2300cm/sec, -1900cm/sec and -2100cm/sec. The agreement between the model and the measurements is better than is first apparent when the error bars for the observations are taken into account: $\pm$1000cm/sec at 300km, $\pm$3500cm/sec at 525km and $\pm$4000cm/sec at 600km.

Another quantity that can be compared with measurement is the H+ flux at 1000km. Evans and Holt (1977) have inferred from measurements at Millstone Hill that in winter "...the [H+] flux remains upward after sunset, but usually becomes downward after midnight until sunrise...". The results from the simulation with the one dimensional model show that the H+ flux below the H+ peak (1000km at t=1 hour) is downward and of the order of $5X10^{6}$ /cm2-sec. Above the peak the flux is upward and about $1.0X10^{7}$ /cm2-sec. The fact that the simulation does not indicate a downward flux at 1000km (the t=0 profile is an after midnight profile) may be due to the fact that the upper boundary condition at 2000km is simply an infinite sink or source of H+ and therefore does not adequately represent the coupling between the night and dayside hemispheres. This coupling along plasma tubes is responsible for the maintenance of the downward H+ flux

at 1000km on winter nights.

IV-3 Aug. 14, 1973 Millstone Hill Profile

Figure IV-4 shows the Aug. 14, 1973 Millstone Hill profile (Evans and Holt, 1977) at 2200 EST. The profile was selected for the simulation because measured profiles at five subsequent times during the night were available (Evans and Holt, 1977). It is characterized by a rather low O+ - H+ transition height: about 800km.

Figure IV-5 shows the profile at t=1 hour. The profiles shown by alternating long and short dashes were measured at Millstone Hill. The height of the H+ peak is at 650km for both the measurements and the simulation. The heights of the F-region peaks are also in good agreement, the simulation peak being about 40km higher. This is understandable in view of the characteristic rise of the F-region peak as the F-region decays during the night. The simulation, however, appears to be "leading", in time, the measured evolution of the profile. The slower decay of the measured profile is possibly due to neutral wind transport of plasma helping to maintain the night-time ionosphere. This processs of neutral wind plasma transport could be added to the FES model in the future, however, it was not included in these simulations. In addtition to the agreement in the altitudes of the peaks, there is excellent

FIGURE IV-4

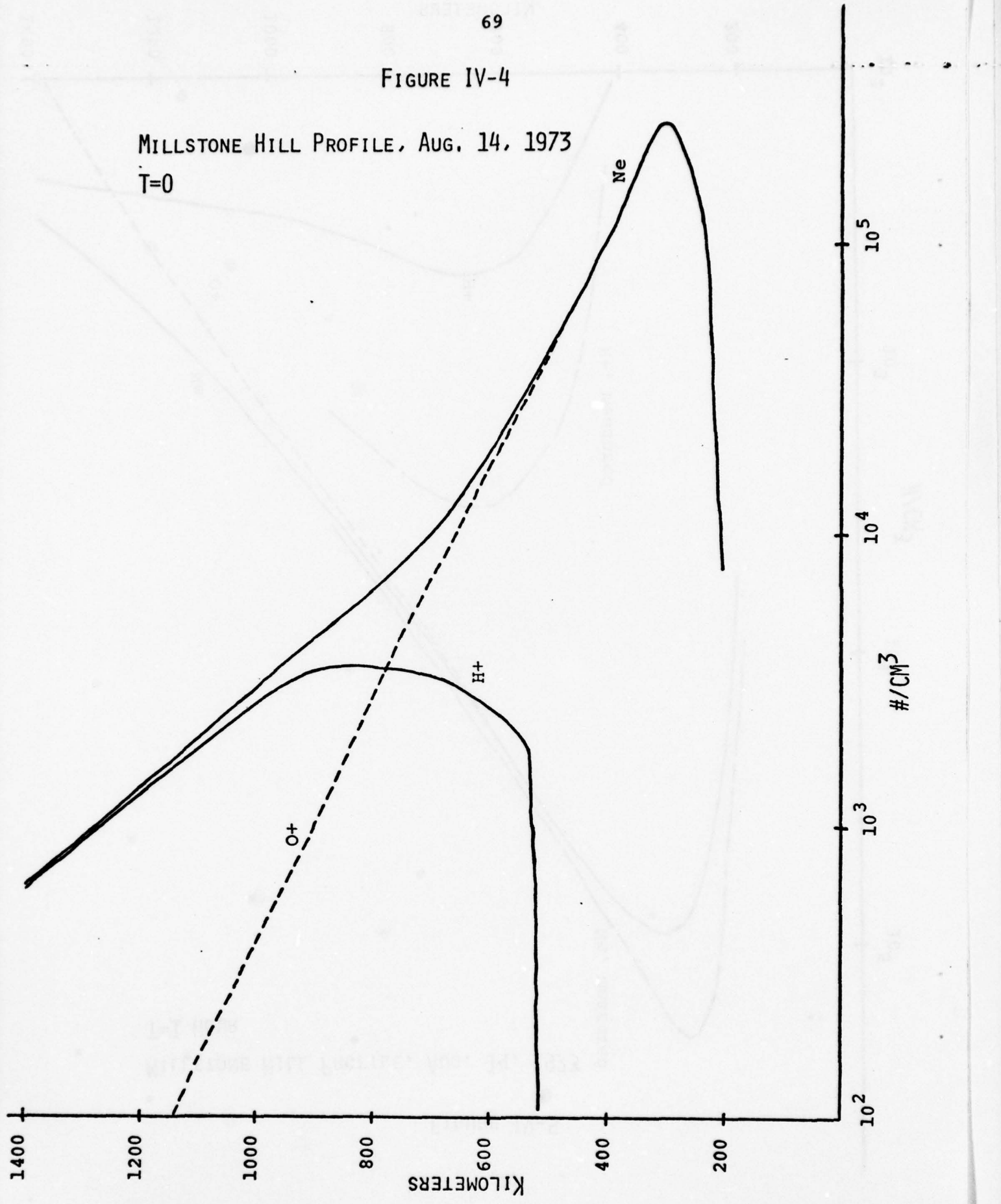
MILLSTONE HILL PROFILE, AUG. 14, 1973
T=0
Ne
H+
O+
10^5
10^4
10^3
10^2
#/CM^3
1400
1200
1000
800
600
400
200
KILOMETERS

FIGURE IV-5

MILLSTONE HILL PROFILE, AUG. 14, 1973
T=1 HOUR

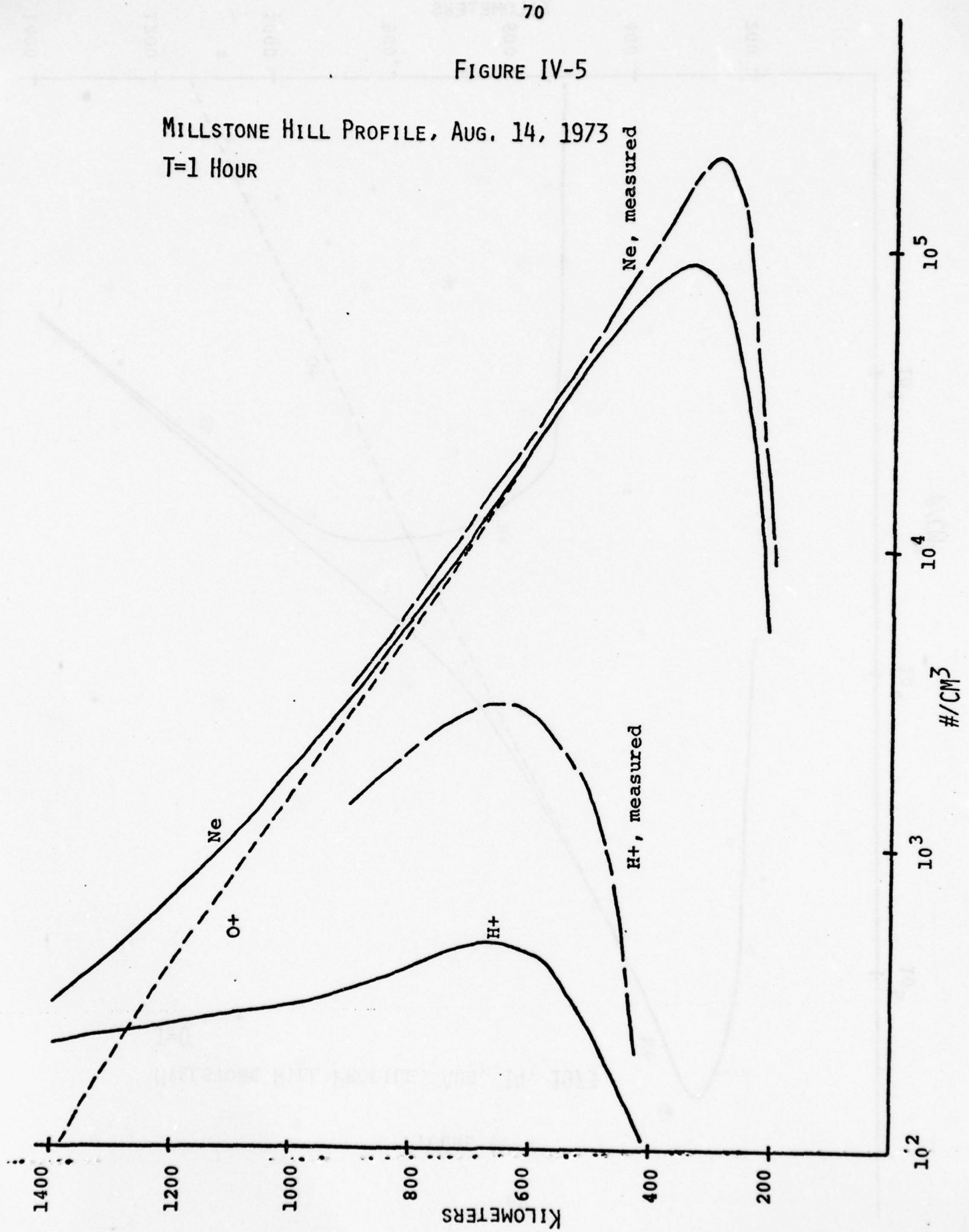

agreement between the shapes of the measured and simulated profiles - in particular the slope of the Ne profile in the top-side F-region. There has been a dramatic change in the O+ - H+ transition height: it moved from 800km at t=0 to almost 1300km at t=1 hour. This will be considered while examining Figure IV-6 which shows the profile at t=3 hours (Millstone Hill 0100 EST Aug. 15, 1973).

In Figure IV-6 the alternately long and short dashed lines represent the measured Millstone Hill profiles. The shape agreement remains excellent at t=3 hours as well as the agreement between the peak heights. The decay rate of the model ionosphere continues to exceed that of the measured - this effect is most noticeable in the case of the H+ profile. The agreement between the Ne profile slopes remains excellent. The O+ - H+ transition height in the simulation is about 1500km though the graph does not show this height. The O+ - H+ transition height for the measured profile is at about 900km - an increase of about 100km since t=0 whereas the simulation shows an increase from 800km to 1500km in the same time span.

Measurements at Millstone were made of the vertical O+ velocity. The values obtained at Millstone Hill and in the simulation at t=3 hours are shown in Table IV-1. The agreement in the flux figures is reasonable especially in

FIGURE IV-6

MILLSTONE HILL PROFILE, AUG. 14, 1973
T=3 HOURS

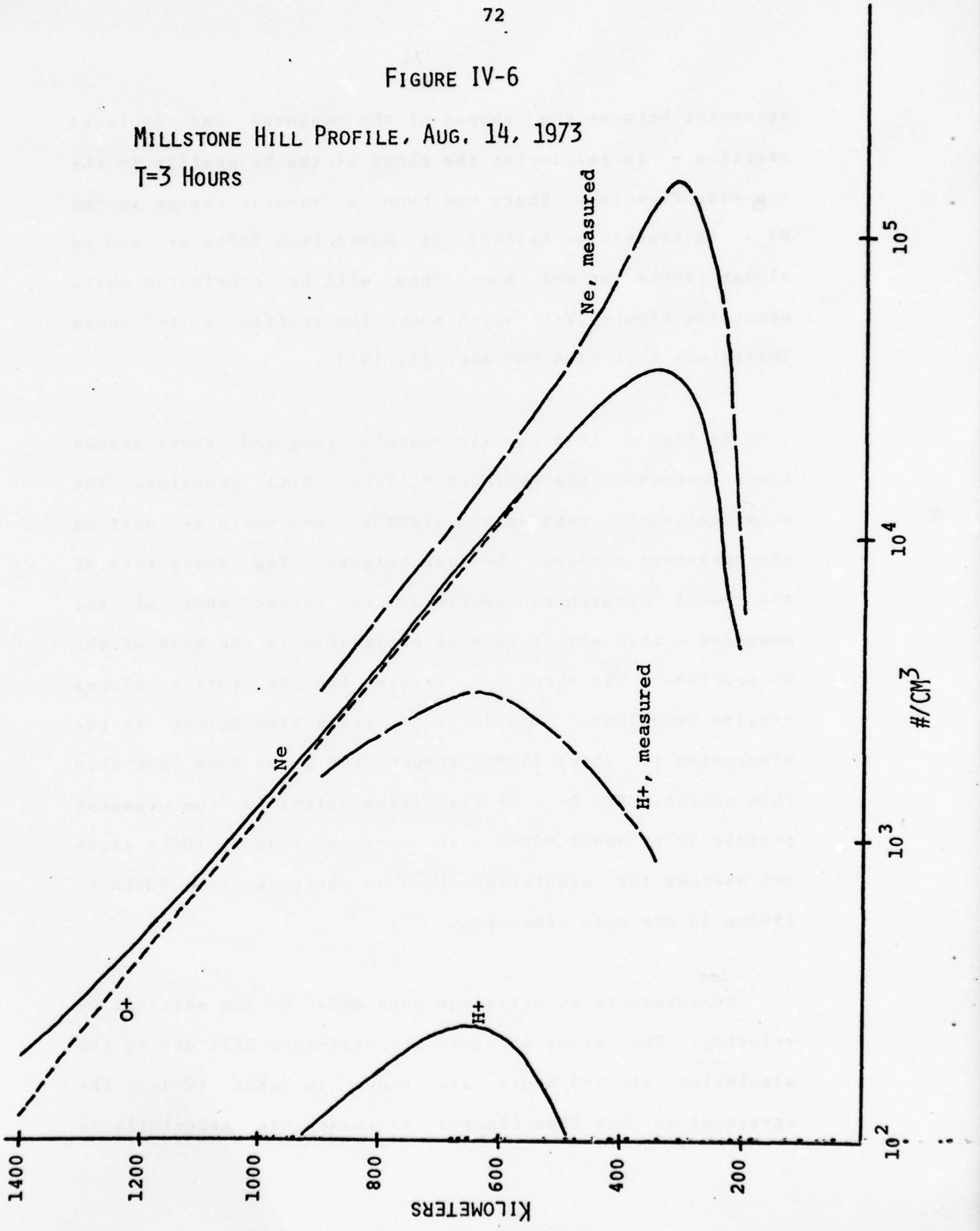

TABLE IV-1

O+ VERTICAL VELOCITY MEASURED AND CALCULATED

Height km	Vertical* Velocity cm/sec Measured	Vertical Velocity cm/sec Calc.	Flux #/cm^2-sec Measured	Flux #/cm^2-sec Calc.
825	-2100	-800	-5.9E6	-2.4E6
750	-1000	-700	-5.1E6	-3.8E6
675	-300	-700	-2.6E6	-5.0E6
600	+200	-800	+3.1E6	-1.0E7
525	+200	-900	+5.7E6	-1.6E7
450	-200	-1400	-1.1E7	-3.8E7

* "+" sign means upward

view of the fact that the error bars in the Millstone Hill measurements are large (for example, at 600km and 525km respectively the uncertainties in the velocity measurements were ±2100cm/sec and ±730cm/sec.). The uncertainties in the measurements at 600km and 525km are large enough that even the direction of O+ movement is in doubt.

At t=1 hour the measured H+ vertical flux at 1000km was $6X10^7$/cm2-sec. At the same time and altitude the simulation produced a value of $2.2X10^7$/ cm2-sec. At t=3 hours the measured value was $1.3X10^7$/cm2-sec and the value resulting from the simulation was also $1.3X10^7$/cm2-sec. The agreement in the upward H+ flux is very good, however, it must be noted that since the flux is the product of the vertical velocity and the concentration, the agreement is somewhat misleading since there is a large discrepancy in H+ concentration at 1000km between the measured and simulated values. In the simulation the flux is maintained by a higher vertical flow velocity and a proportionately smaller concentration.

This discrepancy between the H+ profiles deserves comment. The measured H+ concentration was nearly constant at a height of 650km from t=0 to t=3 hours ($3X10^2$/cm3). On the other hand the H+ profile of the simulation decayed from $3X10^2$/cm3 at t=0 to $2.4X10^2$/cm3 at t=3 hours. For the H+

profile peak to remain in equilibrium for 3 hours requires that the processes of chemical production and loss of H+ + O $\rightleftharpoons$ O+ + H) as well as transport were in balance. The equation

$$P_c - L_c + \Delta T = 0$$

must hold where

P_c is the H+ chemical production rate #/cm3-sec

L_c is the H+ loss rate, #/cm-sec

ΔT is the change in H+ concentration due to transport, #/cm3-sec

It is possible for this equation to hold at a given height for various H+ concentrations. To accommodate this the relative values of P_c L_c and ΔT would be different. This is the crux of the discrepancy concerning the H+ concentration. In the model, simplifications were made that affected the agreement between the simulation and the measured profile: temperature effects were ignored, i.e. neutral,ion, and electron temperatures were independent of time; there were no EXB drifts or neutral wind transport of plasma etc. In addition, the 1000K neutral atmosphere assumed in the model may have been too high for the solar minimum period being considered. A cooler neutral atmosphere would mean,ultimately, that plasma loss would proceed more slowly in the F2 region. These differences between the model and reality, in addition to the uncertainties in the chemical

reaction rates and diffusion coefficients, account for the differences between the measured H+ profile and that of the simulation.

The ionosphere is a very sensitive region of the earth's upper atmosphere and thus subtle changes in the rates of physical processes can make significant differences. What has been suggested, though, is that the FES technique shows promise as a tool to explore the sensitivity of the ionosphere to changes in the rates of these phycsical processes.

Chapter V

Two Dimensional Model

V-1 Introduction

The one dimensional model used in the auroral ionosphere simulations was extended to two spatial dimensions. The reason for this was twofold. First, it achieves a more general model that enables the simulation of phenomena that can be expected to exibit latitudinal variation, and second, there was a specific application that could readily be considered, namely, to attempt to simulate the formation of the poleward wall of the mid-latitude ionospheric trough (Mendillo and Chacko, 1977) by asserting that it is caused by the precipitation of energetic electrons in the auroral zone. Chapter VI discusses and presents the results of this simulation.

V-2 Similarities With The One Dimensional Model

The two dimensional model is a direct extension of the one dimensional model and therefore it has several similarities. In fact, several aspects are exactly the same.

It was decided to not include the latitudinal variation of the neutral atmosphere in the two dimensional model. Consequently, the same neutral atmosphere as was used in the one dimensional model was used throughout the latitude range of the two dimensional.

As described in Chapter II, the FES technique treats chemical reactions in such a way that each cell (as far as chemistry is concerned) is independent of those around it. Therefore the inclusion of additional cells to achieve two dimensional coverage does not at all change the model's handling of chemistry. Furthermore, since the production of (O+,e) pairs due to precipitating auroral electrons was calculated in the same way as the chemical reactions (see Chapter II) this process too is unaffected by the extension to two dimensions.

Several other features of the model were altered substantially enough to warrant specific discussion below.

V-3 Geometry and Dip Angle

Figure V-1 shows the two dimensional geometry used in the model. Also shown (dotted lines) are a few of the earth's magnetic field lines. It is seen in Figure V-1 that the method of extending to two dimensions was to stack additional one dimensional geometries side by side, each

FIGURE V-1

POLEWARD WALL SIMULATION

CELL GEOMETRY

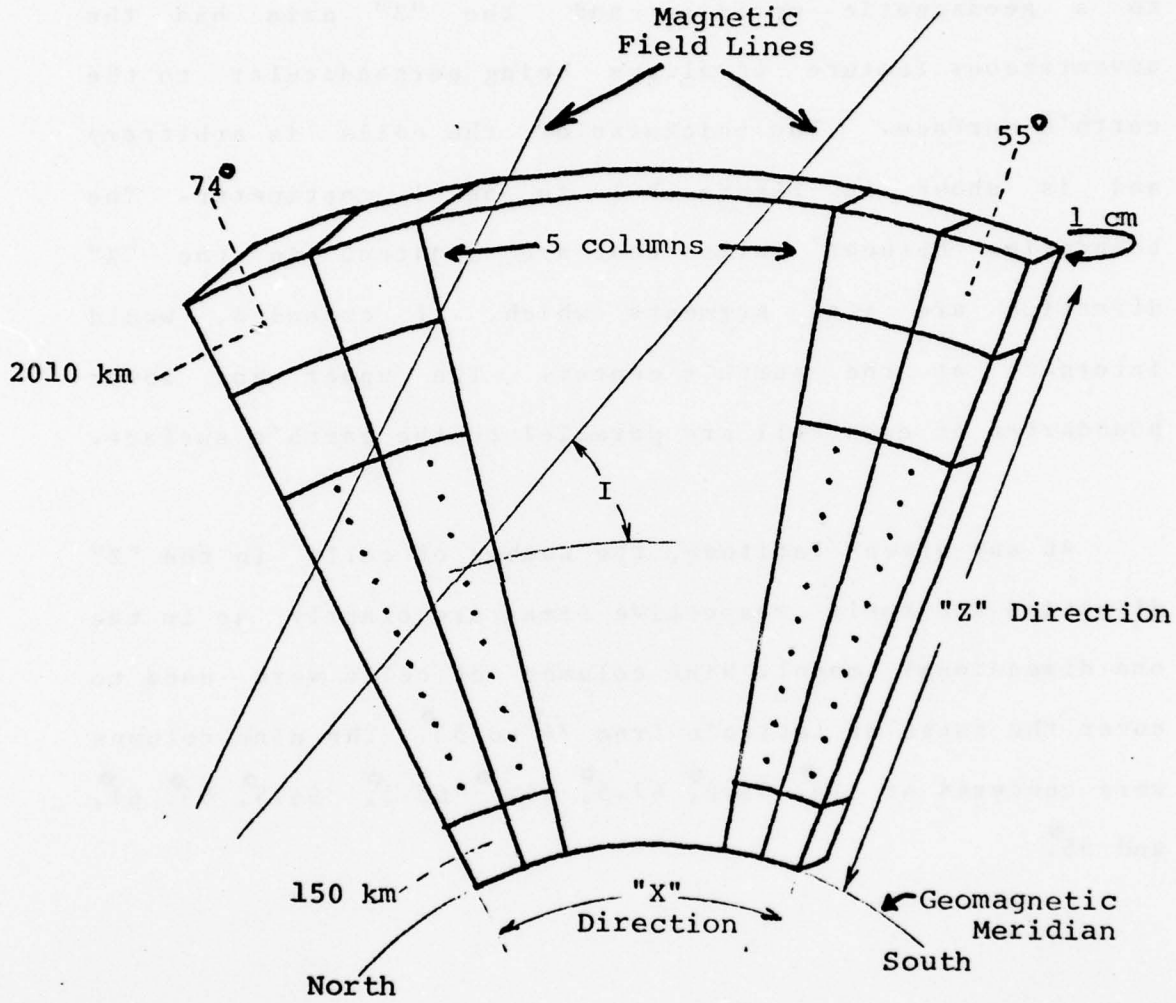

• Earth's Center

with its own geocentric dip angle as this parameter is a function of latitude. The "X" axis of the cells is parallel to a geomagnetic meridian and the "Z" axis has the advantageous feature of always being perpendicular to the earth's surface. The thickness of the cells is arbitrary and is shown in Figure V-1 to be 1 centimeter. The boundaries between cells that are adjacent in the "X" direction are line segments which, if extended, would intersect at the earth's center. The upper and lower boundaries of each cell are parallel to the earth's surface.

At any given latitude, the number of cells in the "Z" direction and their respective sizes are exactly as in the one dimensional model. Nine columns of cells were used to cover the range of latitude from 74° to 55°. The nine columns were centered at 74°, 68.5°, 67.5°, 66.5°, 65.5°, 64.5°, 63°, 61°, and 55°.

V-4 Transport

The transport of H+ and O+ ions due to gravitational drift and concentration gradients is calculated in essentially the same way as in the one dimensional model, see Chapter II. However, there are some complications that must be described.

First, since the model is two dimensional, latitudinal gradients, i.e. in the "X" direction shown in Figure V-1, must be taken into account. This is done by using the formulae presented in Chapter II, but by omitting the term involving the ion scale height (gravitational term) since there is no gravity acting in the "X" direction. There is, though, an additional effect due to the fact that the magnetic field line, in general, will not be aligned with either the "X" or the "Z" axes of the two dimensional geometry. This effect is schematically represented in Figure V-2. In the example illustrated, plasma transport into or out of cell(i,j) across the upper boundary with cell(i,j+1) and the right hand boundary with cell(i+1,j) is being considered.

In the one dimensional model only the upper boundary is relevant and the effect of the dip angle of the magnetic field line is to reduce the amount of vertical plasma transport by the $\sin^2(I)$ factor (see Chapter II). In Figure V-2 it can be seen, however, that the vertical drift velocity due to gravity and vertical concentration gradients may be resolved (after projection onto the magnetic field line along which all plasma is constrained to move - due to the gyro frequency being much greater than the collision frequency) into a vertical and a horizontal component. The vertical component is exactly the same as calculated in the

FIGURE V-2

MAGNETIC FIELD DIP ANGLE
EFFECT ON PLASMA TRANSPORT

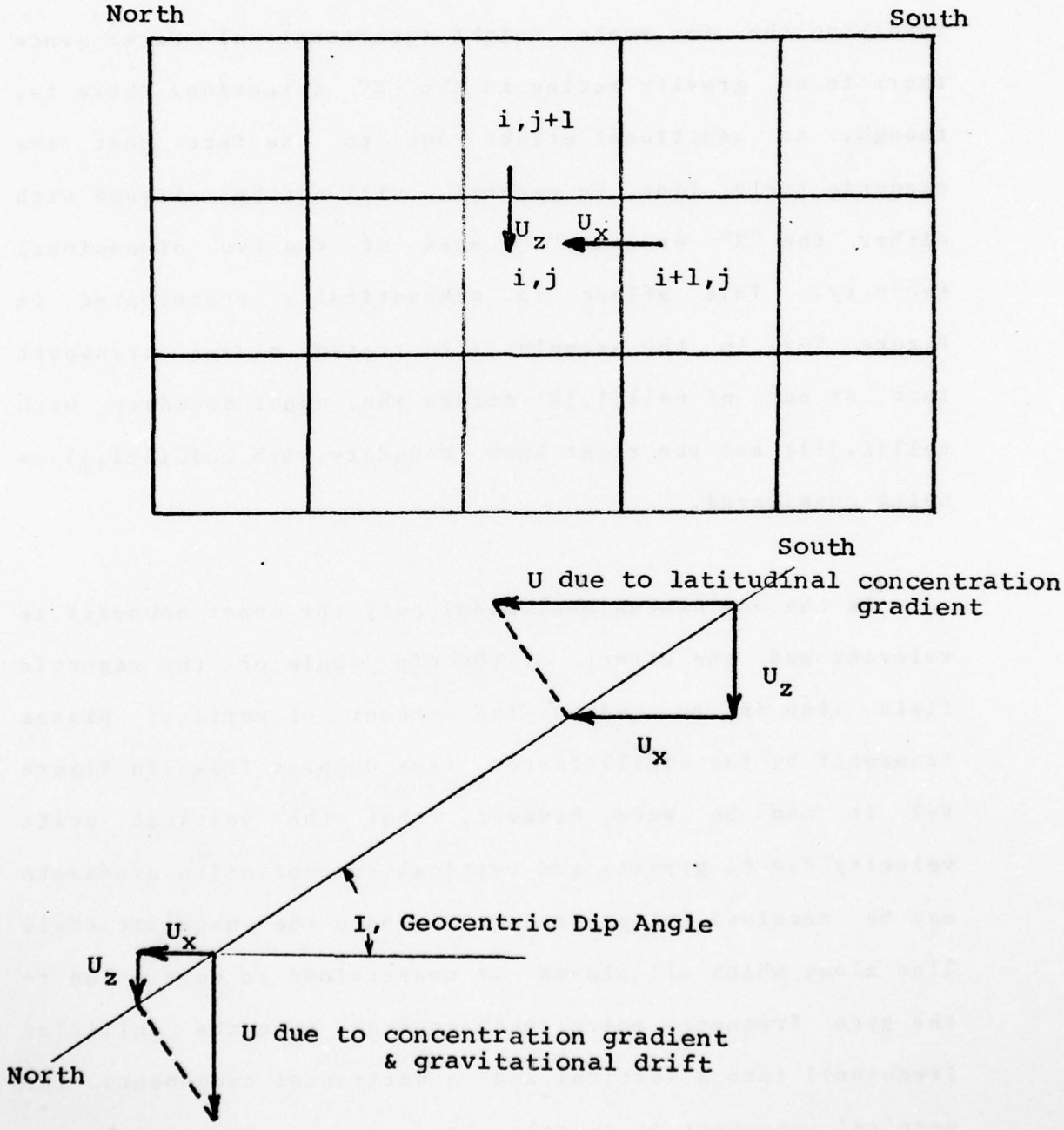

one dimensional case. The horizontal component, which was ignored in the one dimensional model, must be taken into account in the two dimensional. In Figure V-2 the vertical drift velocity resolves into a downward and horizontal drift to the north (left). There is no ambiguity concerning the movement of plasma as a result of the vertical drift component. Material moves from cell(i,j+1) to cell(i,j). This is expected since the gravitational drift velocity was from cell(i,j+1) to cell(i,j) and (in this example) the concentration gradient was calculated between those same two cells. However, what is to be done with horizontal component of the drift velocity? It obviuosly arises from vertical gravitational drift and vertical concentration gradients. Its direction, however, indicates that it moves plasma from cell(i+1,j) into cell(i,j). Interestingly, cell(i+1,j) has not, up to this point, entered into the calculation at all.

This paradox is a direct consequence of the discreet spatial grid. Taken to the limit of infinitesimally small cells one would find the drift velocity at a point in space to be along the magnetic field line. This is consistent with differential equations governing this physical system. As has been stressed though, FES is not explicitly concerned with the differential equations. Therefore, a convention must be adopted to resolve this difficulty that is typical

of those that arise when an essentially continuous process is modeled in a discreet manner. It should be noted, also, that any discreet model would have a similar difficulty and that this current problem is not, then, peculiar to FES.

The convention used is straightforward. Whenever the transport into or out of a given cell(i,j) is considered the concentration gradients across only two boundaries are used; that with cell(i,j+1) and that with cell(i+1,j). If this is done for all cells(i,j) then it is easy to visualize that all boundaries are taken into account and that when the update of plasma concentrations is made after having considered all cells, all transport among adjacent cells has been included.

This convention implies that, in general, (beyond the specific case illustrated in Figure V-2) any vertical drift component moves plasma across the boundary between cells(i,j) and (i,j+1) and that any horizontal drift component moves plasma across the boundary between cells(i,j) and (i+1,j). Thus is preserved the computational convention that when transport into or out of cell(i,j) is considered, transport may occur only across the upper and right hand boundaries. Since the cell sizes used in the model are appropriate for adequate spatial resolution this method yields good results.

V-5 Boundary Conditions

indicated that one dimensional cell geometries were stacked side by side to embody the two dimensional geometry. It was natural, then, to use exactly the same boundary conditions at the top and the bottom of the two dimensional model as were used in the one dimensional (see Chapter II).

The two dimensional model, however, involves two more boundary conditions: those at the northern and southern latitude limits. During the development of the one dimensional model it was learned that care must be taken to assure that, at the higher altitudes, the cells at the extremities of the region do not tend to "fill up" appreciably during the simulation. As already mentioned, in the case of the top cells, this was prevented by using the same boundary conditions as in the one dimensional model.

The boundary conditions used in the two dimensional model at the northern and southern extremeties were the same. What was done was to not allow the plasma concentrations in the columns of cells forming the northern and southern boundaries to change in response to latitudinal plasma transport. The reason that this very simple boundary condition worked is that the latitudinal transport of plasma at the mid and high latitudes (the range of the trough poleward wall simulation) is rather small due to the small

latitudinal concentration gradients and to the orientation of the magnetic field lines. Another reason is that the cells at the northern and southern extremities were made large (10° in extent).

If the model were to be used to simulate the ionosphere in the equatorial region it might be necessary to use a different boundary condition at the latitudinal extremes. This would be necessitated by the orientation of the magnetic field lines which, near the equator, would channel plasma movements in latitudinal directions.

V-6 Calculation Time Step and XMODs

By extending the model to two dimensions an added degree of freedom was given to the process of transport. In the one dimensional model transport, of course, could only occur in the vertical direction, but in the two dimensional it could also occur horizontally. To answer the question - Would the same time steps that were suitable in the one dimensional model also work in the two dimensional? - an XMOD calculation for horizontal transport was made. As expected, the process of horizontal transport is quite slow due to the small latitudinal concentration gradients and to the orientation of the magnetic field lines. Thus horizontal transport could use a longer time step than

vertical transport if desired. It was decided, however, to use the same time step for all transport.

The latitudinal variation of the ionosphere over the range considered in the poleward wall simulation was small enough to permit calculating XMODs for all processes along only one column of cells at a particular latitude. This saved computer time and facilitated the interpretation of the XMODs when checking the stability of the calculation. Had there been a large variation with latitude of important physical parameters, then XMOD calculations would have been necessary at each column of cells to make sure that any instability in the simulation would not go unnoticed.

In summary, then, the same time steps for all processes and at all spatial locations were used in the two dimensional simulation as were used in the one dimensional. These were on the order of one to two seconds.

V-7 Accuracy

Extending the model to two dimensions did not introduce any new sources of error in the simulation nor did it change any. This is one of the advantages of FES. The finite word length of the computer is the primary source of error regardless of the complexity of the model.

AD-A065 551 BOSTON UNIV MASS DEPT OF ASTRONOMY F/G 4/1
FINITE ELEMENT SIMULATION OF PROCESSES IN THE AURORAL IONOSPHER--ETC(U)
JAN 79 B VANCE, M MENDILLO F19628-78-C-0079
UNCLASSIFIED ACBU-SER-III-NO-12 AFGL-TR-79-0003 NL

2 OF 2
AD
AD 65551

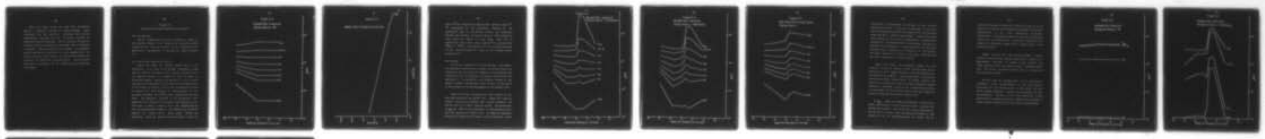

END
DATE
FILMED
5-79
DDC

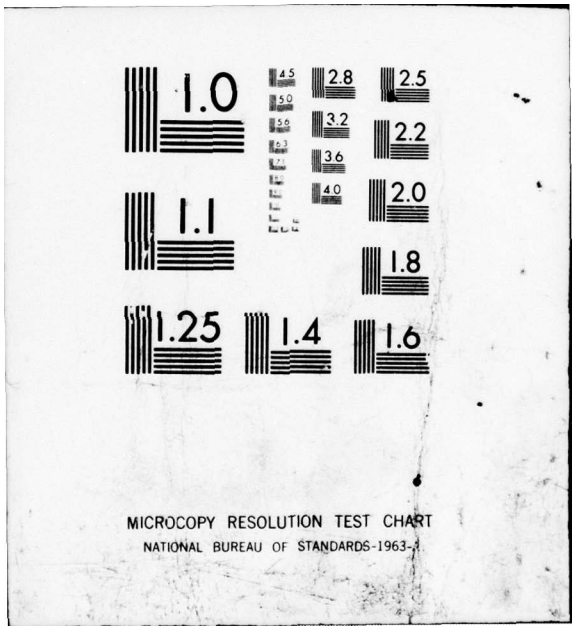
1.0
1.1
1.25
1.4
1.6
1.8
2.0
2.2
2.5
2.8
3.2
3.6
4.0
4.5
5.0
5.6
6.3
7.1
8.0
MICROCOPY RESOLUTION TEST CHART
NATIONAL BUREAU OF STANDARDS-1963-A

This very often is not the case with alternative methods of numerical analysis of complex systems. Those techniques that are explicitly concerned with solving differential equations are not so easily extended to additional spatial dimensions. This is because, frequently, entirely different mathematical algorithms must be developed or adapted. When the algorithms are changed to accommodate greater mathematical complexity it is not uncommon that the overall accuracy of the method will deteriorate beyond that caused by the additional round-off errors. This situation means FES, in principle, has an advantage as no algorithms are changed.

Chapter VI

Mid-Latitude Trough Poleward Wall Simulation

VI-1 Introduction

The two dimensional model was described in detail in the previous chapter. The simulation of the mid-latitude trough poleward wall was selected as an interesting first application. The geometry of the model is shown in Figure V-1.

VI-2 Initial Two Dimensional Profile

Figure VI-1 shows the initial profile used in the simulation. It is based on the average ionospheric trough found by Mendillo and Chacko (1977) during a period of very low magnetic activity in December of 1971. In order to investigate whether particle precipitation in the auroral zone could be responsible for the shape of the poleward wall of the trough, the initial profile was established as shown in Figure VI-1 with constant Ne concentrations at all latitudes northward of 64.5° Corrected Geomagnetic Latitude (CGL). The simulation employed an O+ ion-electron pair production rate typical for the auroral zone (Knudsen et al, 1977) that is shown in Figure VI-2. The expectation was that the characterisitc shape of the poleward wall found by Mendillo and Chacko (1977) would emerge during the simulation. Since the poleward wall was found to occur at

FIGURE VI-1

POLEWARD WALL SIMULATION

TOPSIDE PROFILE, T=0

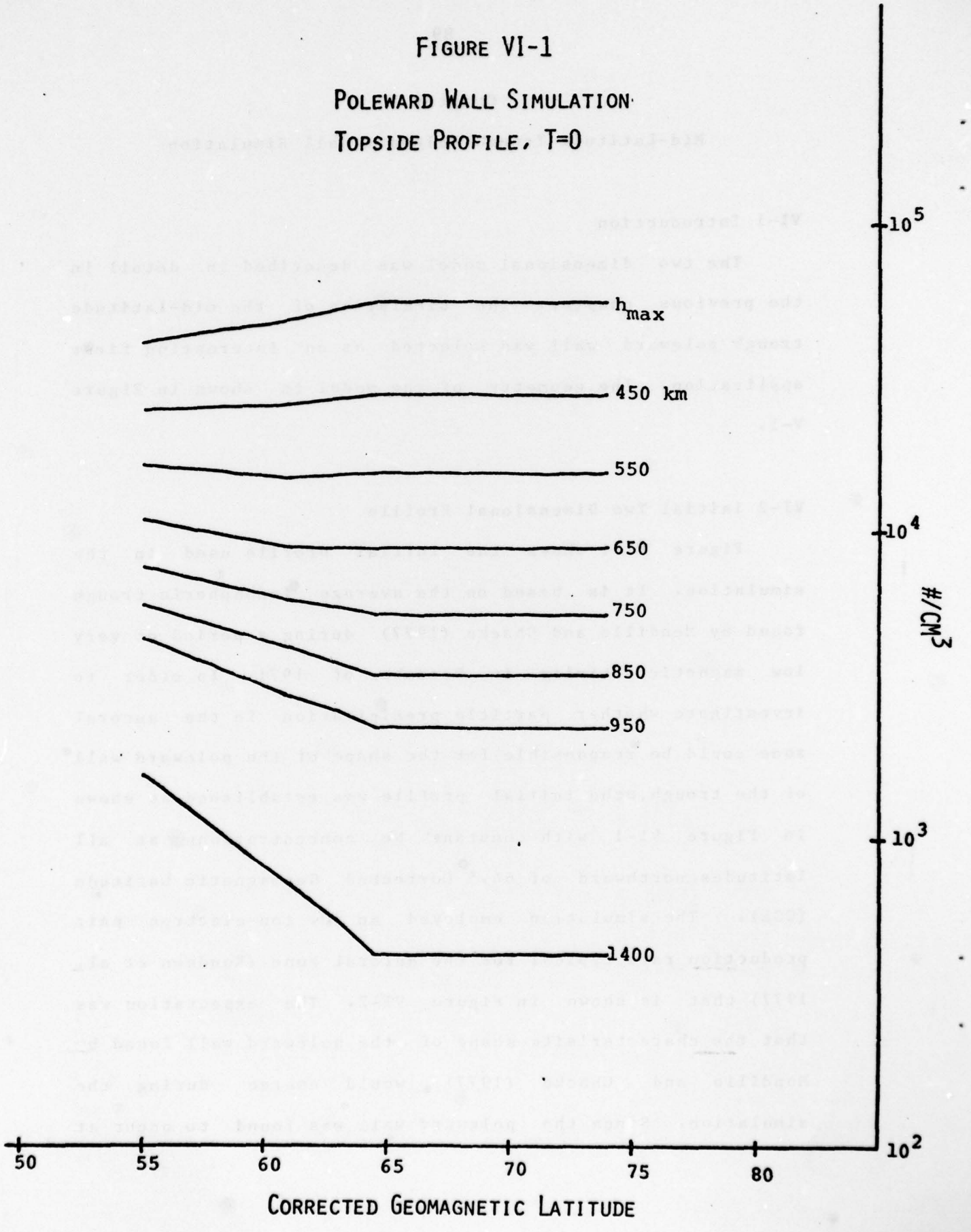

FIGURE VI-2

AURORAL ZONE O+ PRODUCTION FUNCTION

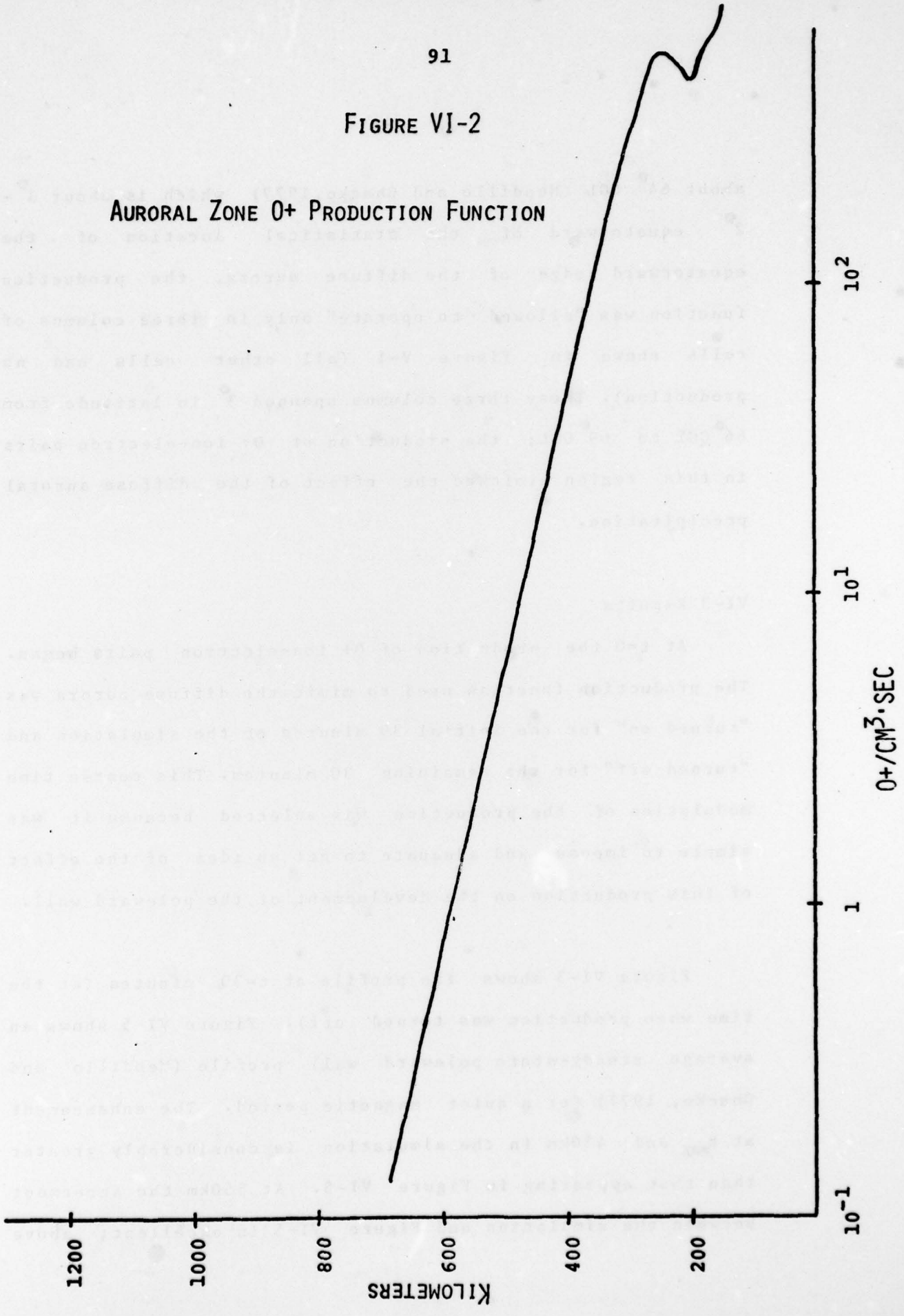

about 64° CGL (Mendillo and Chacko, 1977) which is about 1°-2° equatorward of the statistical location of the equatorward edge of the diffuse aurora, the production function was "allowed to operate" only in three columns of cells shown in Figure V-1 (all other cells had no production). These three columns spanned 3° in latitude from 66° CGL to 69° CGL; the production of O+ ion-electron pairs in this region mimicked the effect of the diffuse auroral precipitation.

VI-3 Results

At t=0 the production of O+ ion-electron pairs began. The production function used to mimic the diffuse aurora was "turned on" for the initial 30 minutes of the simulation and "turned off" for the remaining 30 minutes. This coarse time modulation of the production was selected because it was simple to impose and adequate to get an idea of the effect of this production on the development of the poleward wall.

Figure VI-3 shows the profile at t=30 minutes (at the time when production was turned off). Figure VI-5 shows an average steady-state poleward wall profile (Mendillo and Chacko, 1977) for a quiet magnetic period. The enhancement at h_{MAX} and 450km in the simulation is considerably greater than that appearing in Figure VI-5. At 550km the agreement between the simulation and Figure VI-5 is excellent; above

FIGURE VI-3

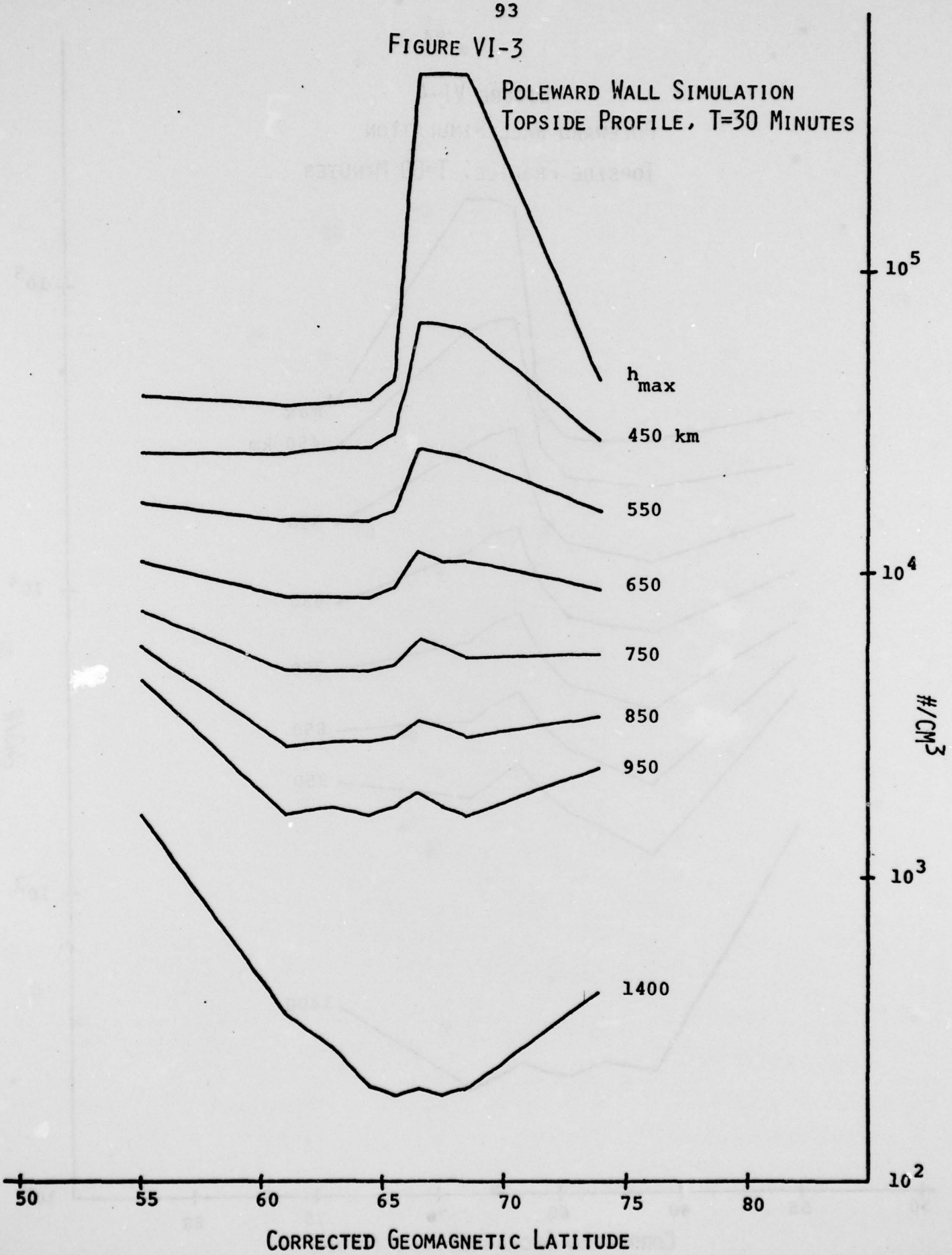
POLEWARD WALL SIMULATION
TOPSIDE PROFILE, T=30 MINUTES
h_{max}
450 km
550
650
750
850
950
1400
10^5
10^4
10^3
10^2
#/CM3
50
55
60
65
70
75
80
CORRECTED GEOMAGNETIC LATITUDE

FIGURE VI-4

POLEWARD WALL SIMULATION

TOPSIDE PROFILE, T=60 MINUTES

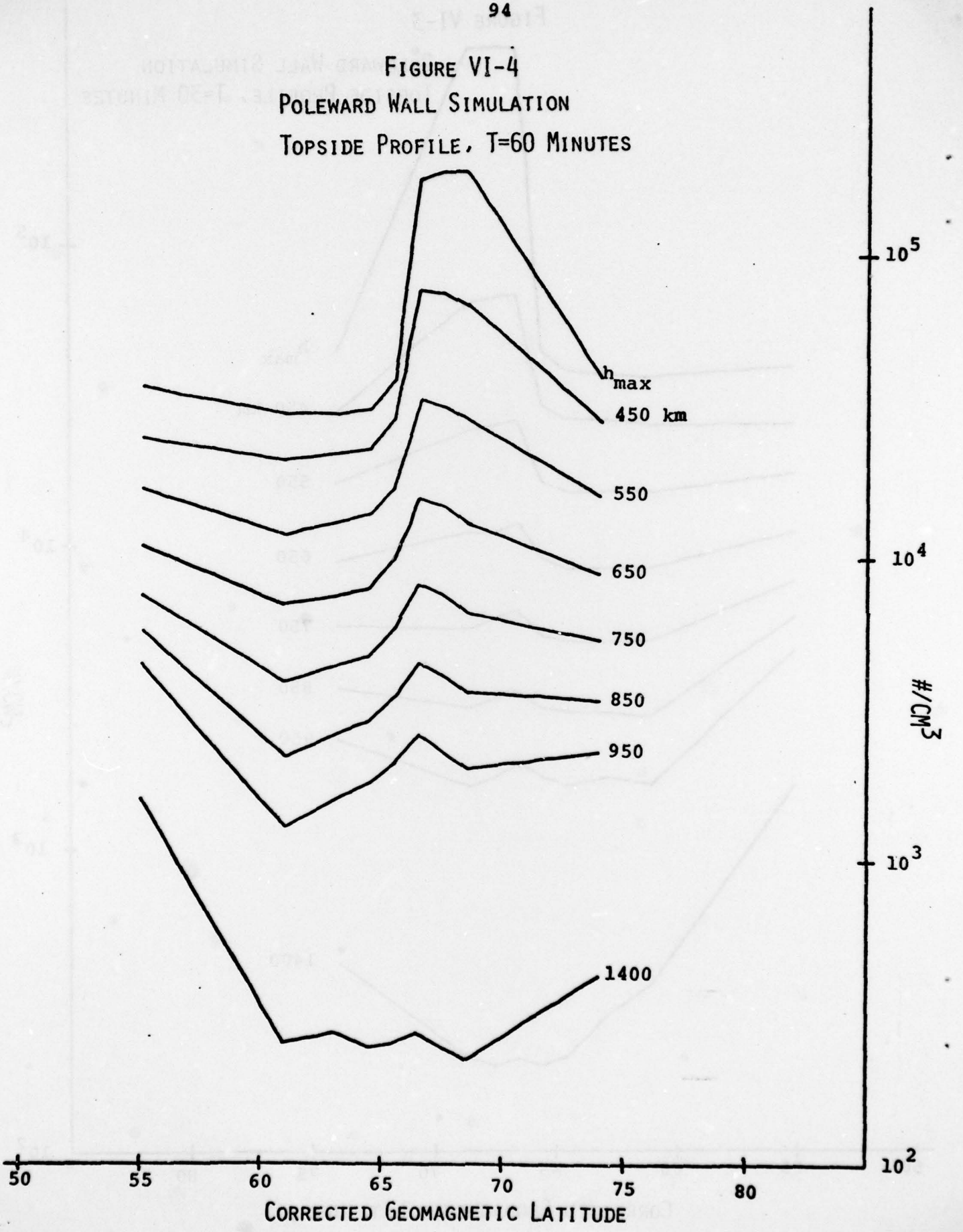

FIGURE VI-5

BASE LEVEL MID-LATITUDE TROUGH

TOPSIDE PROFILE

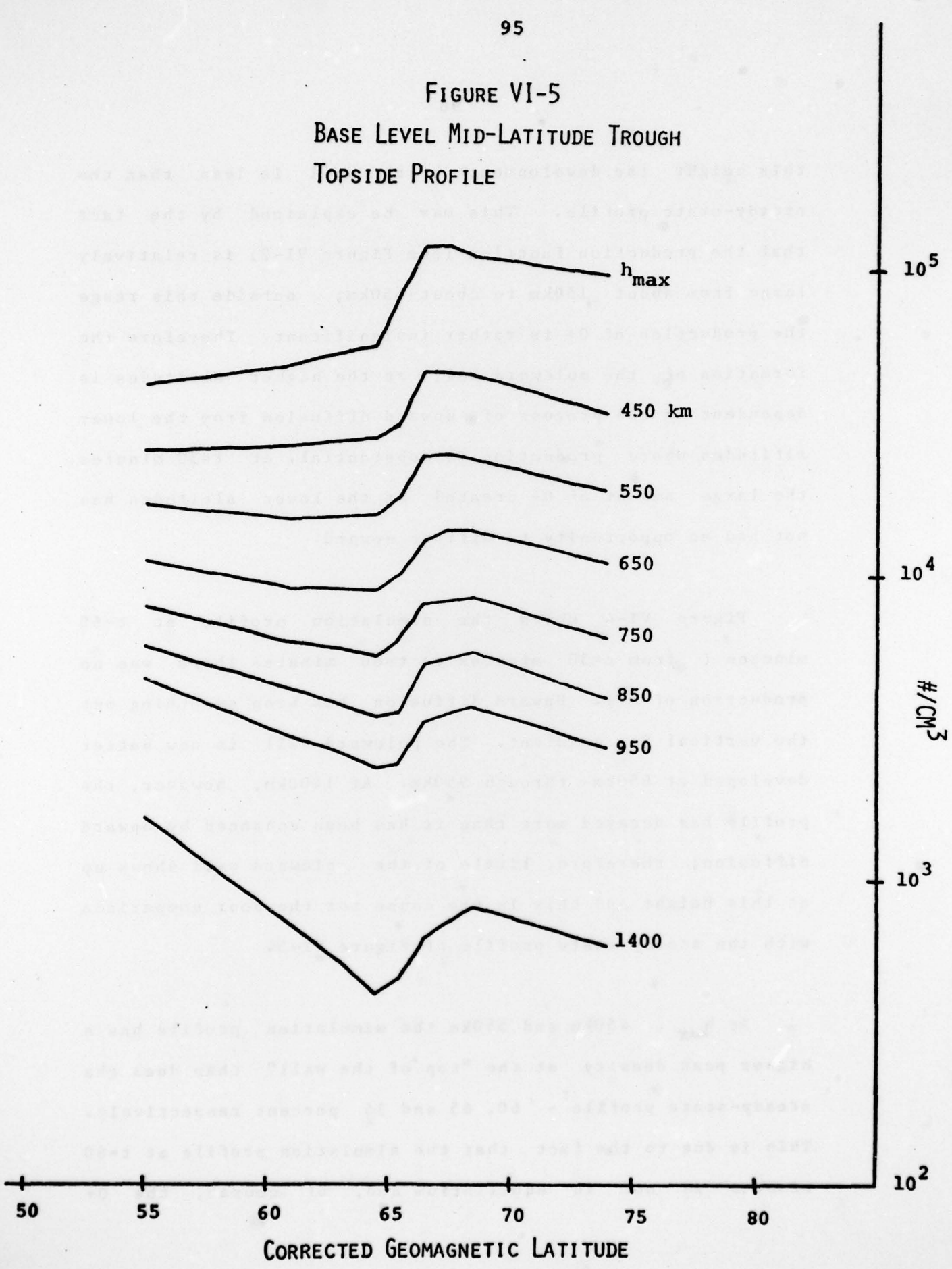

this height the development of the wall is less than the steady-state profile. This may be explained by the fact that the production function (see Figure VI-2) is relatively large from about 150km to about 450km; outside this range the production of O+ is rather insignificant. Therefore the formation of the poleward wall at the higher altitudes is dependent on the process of upward diffusion from the lower altitudes where production is substantial. At t=30 minutes the large amount of O+ created at the lower altitudes has not had an opportunity to diffuse upward.

Figure VI-4 shows the simulation profile at t=60 minutes (from t=30 minutes to t=60 minutes there was no production of O+). Upward diffusion has been smoothing out the vertical Ne gradient. The poleward wall is now better developed at 650km through 950km. At 1400km, however, the profile has decayed more than it has been enhanced by upward diffusion; therefore, little of the poleward wall shows up at this height and this is the cause for the poor comparison with the steady-state profile of Figure VI-5.

At h_{max} , 450km and 550km the simulation profile has a higher peak density at the "top of the wall" than does the steady-state profile - 60, 65 and 36 percent respectively. This is due to the fact that the simulation profile at t=60 minutes is not in equilibrium and, of course, the O+

production function of Figure VI-2 that was turned on for 30 minutes and then off for 30 minutes is probably not the best approximation to the real steady-state condition. Nevertheless, the agreement between the average steady-state profile and the simulation is rather good especially with respect to the general slope of the poleward wall at the various altitudes.

Figure VI-6 and VI-7 show the bottomside F region profile at t=0 and t=60 minutes respectively. There are no measurements with which to compare as the Mendillo and Chacko analysis (1977) was based on Isis 2 topside sounder data. The initial bottomside profile shown in Figure VI-6 was arbitrarily chosen.

The fact that the poleward wall of the mid-latitude ionospheric trough is attributable to the precipitation associated with the diffuse aurora is well known and this finite element simulation supports the plausibility of such an explanation. The hope is that the flexibility of FES (particularly the ease with which a model may be extended to another spatial dimension) has been further demonstrated.

FIGURE VI-6

POLEWARD WALL SIMULATION

BOTTOMSIDE PROFILE, T=0

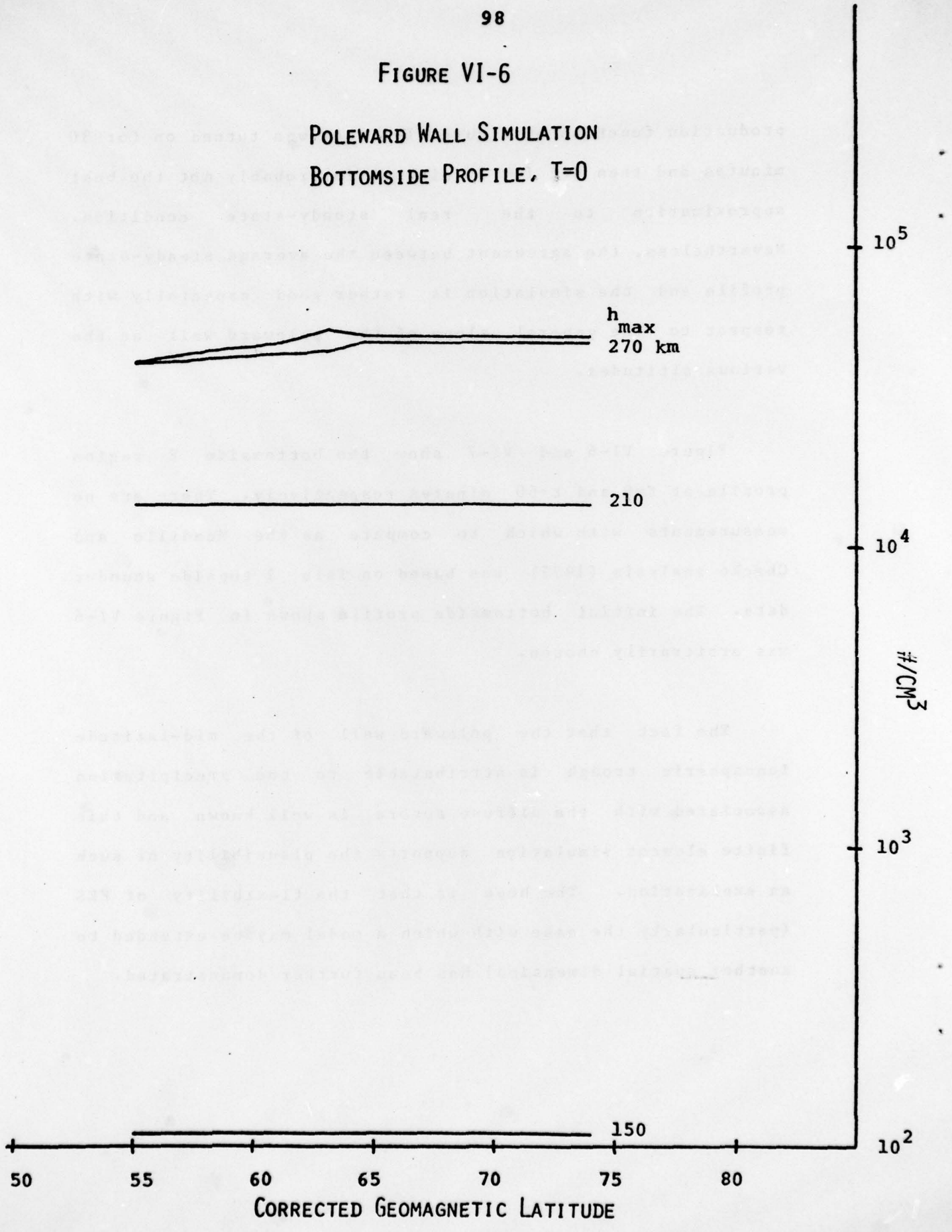

FIGURE VI-7

POLEWARD WALL SIMULATION

BOTTOMSIDE PROFILE, T=60 MINUTES

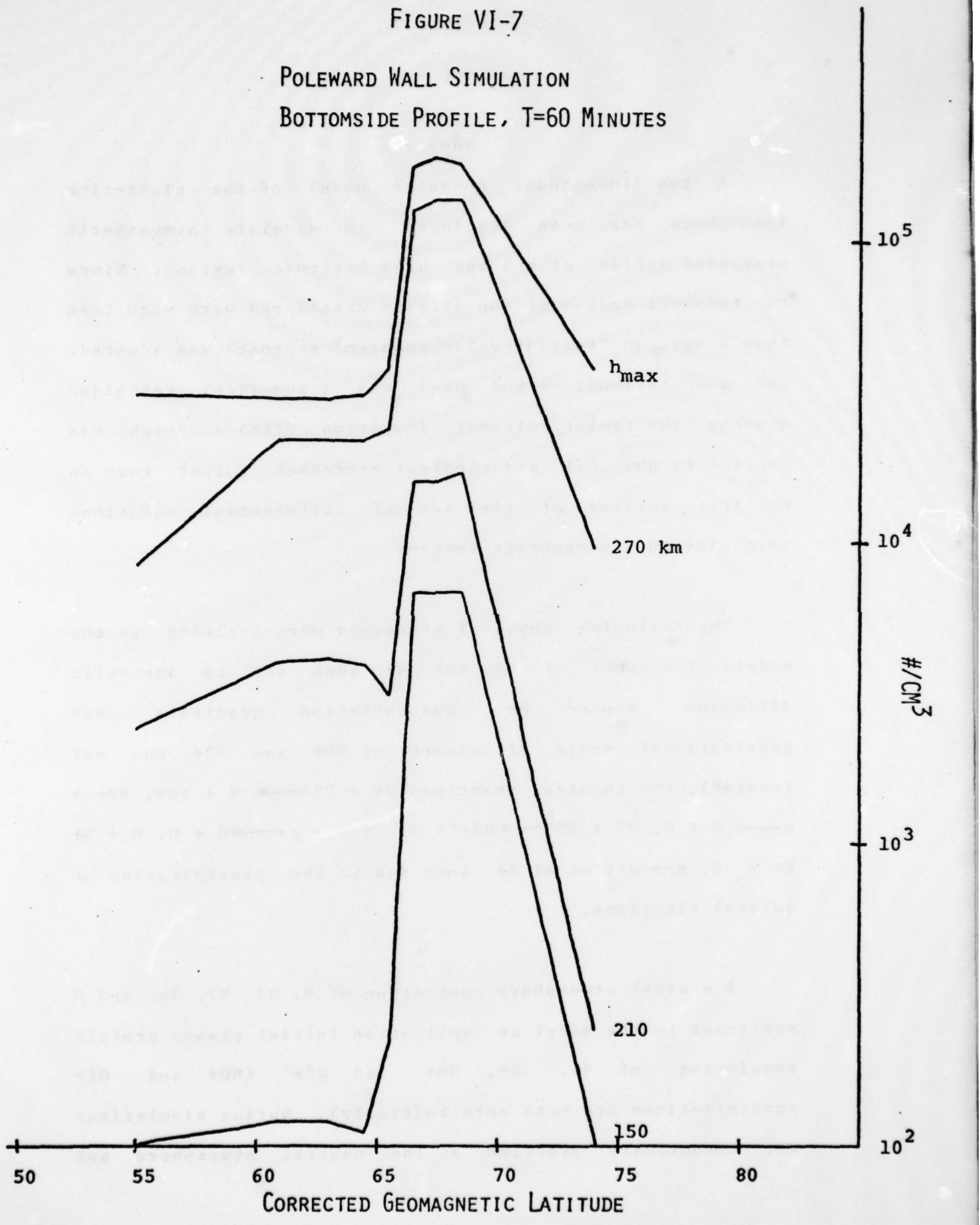

Summary

A two dimensional computer model of the night-time ionosphere has been developed to simulate atmospheric processes acting at mid and high latitude regions. Since the temporal scales of the effects considered were much less than a day, an "initial value problem" approach was adopted. The computational method used was a numerical technique whereby the finite element simulation (FES) approach was applied to physical and chemical processes, rather than an explicit solving of the set of differential equations governing the ionospheric system.

The following physical processes were included in the model: transport of O+ and H+ ions due to ambipolar diffusion caused by concentration gradients and gravitational drift (transport of NO+ and O2+ was not treated), the chemical reactions $O^+ + N_2 \longrightarrow N + NO^+$, $NO^+ + e \longrightarrow N + O$, $O^+ + O_2 \longrightarrow O_2^+ + O$, $O_2^+ + e \longrightarrow O + O$, $H + O^+ \longrightarrow H^+ + O$, production of O+ ions due to the precipitation of auroral electrons.

A neutral atmosphere consisting of O, O2, N2, He, and H was input to the model as well as an initial plasma profile consisting of H+, O+, NO+ and O2+ (NO+ and O2+ concentrations are both zero initially). During simulations the temperature profiles of the neutral atmosphere and

plasma did not change (electron temperature was everywhere equal to twice the ion temperature which was everywhere equal to the neutral temperature). Furthermore, the concentration profile of the neutral atmosphere was considered essentially time independent.

The cell geometry was an array of "wedge" shaped cells with northern and southern boundaries formed by rays drawn from the earth's center. The upper and lower boundaries of each cell were arcs drawn with a geocentric center. The two spatial dimensions covered by this geometry were altitude (from 150km to 2000km) and latitude (for the poleward wall simulation the latitudinal extent of the array was about 20°). The north-south axis of the array was colinear with a geomagnetic meridian. Suitable boundary conditions for physical processes were used at the extremities of the array. In altitude thickness the cells ranged from 20km to 100km at low and high altitudes respectively.

When a simulation was made the initial profiles (neutral and plasma) were input and the time evolution of the concentrations of O+, H+, NO+, and O2+ was calculated for each cell. This was carried out using a suitable time step for each process and updating the ion concentrations in response to chemical and transport effects.

A one dimensional (height-dependent) version of the code was used to simulate the ionosphere beneath the mid-winter dayside auroral cusp (effectively a night-time ionosphere). The one dimensional code was also used to simulate the behavior of night-time Millstone Hill profiles. A two dimensional (height and latitude) simulation was carried out for the mid-latitude ionospheric trough and poleward wall region. In each case, the simulations spanned a 2-3 hour time period.

This work has shown the flexibility of the FES technique and its suitability for computer modeling studies of ionospheric processes and effects. In the future, temperature effects and electrodynamic drifts could be added in order to achieve a more realistic model. Beyond these two processes, the effects of neutral wind plasma transport and additional chemical reactions might also be included. Finally, an extended model (including the additional processes mentioned above) could be expanded to 3 spatial dimensions to realize the most general model possible.

REFERENCES

Balko, B., and Mendillo, M. (1977). Finite Element Simulation Applied to the Transport of Neutral and Ionized Particles in the Earth's Upper Atmosphere. Astronomical Contributions Boston University Series III, No.1.

Banks, P.M., Holzer, T.E. (1969). Features of Plasma Transport in the Upper Atmosphere. Journal of Geophysical Research 74,6304.

Banks, P.M., and Kockarts, G. (1973). Aeronomy Part A and Aeronomy Part B. Academic Press, New York.

Chacko, C. and Mendillo, M. (1977). Electron Density Enhancements in the F Region Beneath the Magnetospheric Cusp. Journal of Geophysical Research 82, 4757.

Evans, J.V. and Holt, J.M. (1977). Nighttime Proton Fluxes at Millstone Hill. MIT Lincoln Laboratory, NSF Grant ATM75-22193.

Hastings, J.T. and Roble, R.G. (1977). An Automatic Technique for Solving Coupled Vector Systems of Non-Linear Parabolic Partial Differential Equations in One Space Dimension. Planetary and Space Science 25, 209.

Knudsen, W.C. et al (1977). Numerical Model of the Convecting F2 Ionosphere at High Latitudes. Journal of Geophysical Research 82, 4784.

Mendillo, M. and Chacko, C. (1977). The Baselevel Ionospheric Trough. Journal of Geophysical Research 82, 5129.

Rishbeth, H. and Garriott, O.K. (1969). Introduction to Ionospheric Physics. Academic Press, New York.